

Published in final edited form as:

Nat Neurosci. 2019 January ; 22(1): 106–119. doi:10.1038/s41593-018-0288-9.

GABA and glutamate neurons in the VTA regulate sleep and wakefulness

Xiao Yu^{#1}, Wen Li^{#2}, Ying Ma¹, Kyoko Tossell¹, Julia J. Harris^{1,3}, Edward C. Harding¹, Wei Ba¹, Giulia Miracca¹, Dan Wang², Long Li², Juan Guo², Ming Chen⁴, Yuqi Li¹, Raquel Yustos¹, Alexei L. Vyssotski⁵, Denis Burdakov³, Qianzi Yang², Hailong Dong^{2,*}, Nicholas P. Franks^{1,6,7,*}, and William Wisden^{1,6,7,*}

¹Department of Life Sciences, Imperial College London, London, U.K. ²Department of Anesthesiology & Perioperative Medicine, Xijing Hospital, Xi'an, Shanxi, China ³The Francis Crick Institute, London, UK ⁴iHuman Institute, ShanghaiTech University, Shanghai, China ⁵Institute of Neuroinformatics, University of Zürich/ETH Zürich, Switzerland ⁶Centre for Neurotechnology, Imperial College London, London, U.K ⁷UK Dementia Research Institute, Imperial College London, London, U.K.

These authors contributed equally to this work.

Abstract

We screened for novel circuits in the mouse brain that promote wakefulness. Chemogenetic activation experiments and EEG recordings pointed to glutamatergic/nitroergic (NOS1) and GABAergic neurons in the VTA. Activating glutamatergic/NOS1 neurons, which were wake- and REM-sleep-active, produced wakefulness through projections to the nucleus accumbens and the lateral hypothalamus. Lesioning the glutamate cells impaired the consolidation of wakefulness. By contrast, activation of GABAergic VTA neurons elicited long-lasting NREM-like sleep resembling sedation. Lesioning these neurons produced an increase in wakefulness that persisted for at least 4 months. Surprisingly, these VTA GABAergic neurons were wake- and REM-sleep-active. We suggest that GABAergic VTA neurons may limit wakefulness by inhibiting the arousal-promoting VTA glutamatergic and/or dopaminergic neurons and through projections to the lateral hypothalamus. Thus, in addition to its contribution to goal- and reward-directed behaviours, the VTA has a role in regulating sleep and wakefulness.

*Correspondence: w.wisden@imperial.ac.uk, n.franks@imperial.ac.uk or hldong6@hotmail.com.

Reporting Summary. Further information on research design is available in the Life Sciences Reporting Summary linked to this article.

Data availability statement

The datasets generated during and/or analyzed during the current study are available from the corresponding authors on reasonable request.

Author contributions

N.P.F. and W.W. conceived, and with X.Y. and H.D. designed the experiments, X.Y., W.L., Y.M., K.T., J.J.H., E.C.H., W.B., G.M., D.W., L.L., J.G., M.C., Y.L., R.Y., D.B. and Q. Y. performed the experiments and/or data analysis, A.L.V. provided the Neurologgers, N.P.F. and W.W. contributed to the data analysis and with H.D. supervised the project. N.P.F., X.Y. and W.W. wrote the paper.

Competing interests

The authors declare no competing interests.

We still do not know all the circuitry in mammals regulating wakefulness and sleep^{1–4}. Broadly, wakefulness is promoted by ascending aminergic and peptidergic systems^{1,5–8}. GABAergic and glutamatergic pathways can also induce wakefulness and physical activity^{9–17}. On the other hand, sleep is promoted by GABAergic/peptidergic and glutamatergic/nitroergic neurons that inhibit the wake-promoting neurons^{3,18–23}.

Here, we describe a non-hypothesis driven chemogenetic search for further circuitry controlling vigilance states, and unexpectedly converge on the ventral tegmental area (VTA). The VTA is intensively investigated for its regulation of goal-, and reward-directed and social behaviors^{24–28}. As well as dopamine neurons (VTA^{DA}), the VTA contains GABAergic and glutamatergic neurons, which independently project out of the VTA^{24,29,30}. These GABA and glutamate neurons are believed to control reward-, goal-directed and social behaviour^{31,32}. These behaviours require wakefulness, and indeed VTA^{DA} neurons are selectively wake and REM-sleep active, and actually promote wakefulness^{5,8,33}. Complimenting this work, we find that VTA glutamate/NOS1 and GABA neurons increase and decrease wakefulness respectively. The VTA is, therefore, a node whose circuitry potently influences vigilance state.

Results

A chemogenetic search for glutamatergic circuitry enhancing wakefulness

We searched for glutamatergic neurons in the posterior hypothalamic/midbrain area (PH/MB) that could promote wakefulness (Fig. 1). By injecting AAV-DIO-hM3Dq-mCherry into *Vglut2-ires-Cre* mice, we expressed the excitatory hM3Dq DREADD receptor in *Vglut2* neurons in progressively more defined locations (Fig. 1). [note: for the following series of experiments, CNO (1 mg/kg) was injected *i.p.* at the start of “lights on”, when the mice had their maximal sleep drive. Injecting CNO (1 mg/kg) *i.p.* into AAV-naïve *Vglut2-ires-Cre* mice - *i.e.* mice not injected with AAV - did not produce any changes in the amounts of sleep or wakefulness (Supplementary Fig. 1a)].

We obtained dramatic results from large volume injections of AAV-DIO-hM3Dq-mCherry into the PH/MB of *Vglut2-ires-Cre* mice [(PH/MB)_L^{*Vglut2*}-hM3Dq mice] (Fig. 1a). Following CNO injections, 100% wakefulness was induced for 12 hours compared with saline-injected control mice (Fig. 1b, c). In these (PH/MB)_L^{*Vglut2*}-hM3Dq mice, hM3Dq-mCherry receptor expression (determined by mCherry staining) was found throughout the lateral hypothalamus (LH), dorsal medial hypothalamus (DMH), ventral medial hypothalamus (VMH), mammillary area (MM), tuberomammillary (TMN) area, supramammillary area (SuM), VTA and interpeduncular nucleus (IPN). A smaller AAV injection volume into the PH/MB of *Vglut2-ires-Cre* mice resulted in hM3Dq expression in the LH, MM and VTA (PH/MB)_S^{*Vglut2*}-hM3Dq mice, Fig. 1d). CNO *i.p.* injection into these (PH/MB)_S^{*Vglut2*}-hM3Dq mice produced continuous wakefulness for approximately 5 hours, followed by enhanced wakefulness for another 7 hours (Fig. 1e, f). Restricting hM3Dq expression to the LH and activating with systemic CNO also produced extended wakefulness (Fig. 1g, h, i).

By contrast, restricting hM3Dq expression to glutamatergic neurons in the mammillary area of *Vglut2-ires-Cre* mice (Fig. 1j, Supplementary Fig. 2a, M *Vglut2*-hM3Dq mice), and giving CNO did not produce arousal above that resulting from baseline saline injections (Fig. 1k, l). Restricting hM3Dq receptor expression to the IPN of *Vglut2-ires-Cre* mice (Fig. 1m, Supplementary Fig. 2b, IPN *Vglut2*-hM3Dq mice), and subsequent injection of CNO also did not elicit arousal compared with saline injection (Fig. 1n, o).

Glutamatergic neurons in the VTA produce wakefulness

We next limited hM3Dq receptor expression to the VTA of *Vglut2-ires-Cre* mice to make VTA *Vglut2*-hM3Dq mice (Fig. 1p, Supplementary Fig. 2c). Following 1 mg/kg CNO *i.p.* injection, there was 5 hours of 100% wakefulness; the extent of wakefulness remained elevated for nearly the entire “lights on” period (Fig. 1q, r). [note: as a further control for the specificity of CNO’s actions, we injected AAV-DIO-mCherry into the VTA of *Vglut2-ires-Cre* mice; CNO injection (*i.p.*) into these VTA *Vglut2*-mCherry mice had no effect on the amounts of sleep or wakefulness (Supplementary Fig. 1c)].

Of the brain regions that we injected, the VTA *Vglut2* population that promotes wakefulness had not previously been identified in this role, and so we decided to study these cells in detail. We first confirmed that these neurons were excited by CNO in VTA *Vglut2*-hM3Dq mice. One hour after CNO *i.p.* injection into VTA *Vglut2*-hM3Dq mice, cFOS protein was elevated in hM3Dq-expressing VTA *Vglut2* neurons (saline: 41 ± 4 , CNO: 378 ± 36 cFOS-positive cells), confirming excitation of VTA *Vglut2* neurons (Supplementary Fig. 2d). Looking at the CNO-evoked EEG spectra of VTA *Vglut2*-hM3Dq mice (Supplementary Fig. 2e), the excitation of VTA *Vglut2* neurons produced higher theta (8 Hz) activity (Supplementary Fig. 2f) but the EMG signal did not change (Supplementary Fig. 2f). Activation of VTA *Vglut2* neurons also strongly increased the latency to both NREM and REM sleep (Supplementary Fig. 2g). However, excitation of VTA *Vglut2* neurons did not cause hyperactivity (Supplementary Fig. 2h). In an open field assay, the CNO-injected (*i.p.*) mice did not move further than saline-injected mice, but stayed awake for an extended period.

Confirming the behavioral effects of the chemogenetic activation of VTA *Vglut2* neurons, optogenetic activation of VTA *Vglut2* neurons with ChR2 also increased wakefulness (Supplementary Fig. 3a, 3b, c).

VTA *Vglut2* neurons consolidate wakefulness during the sleep-wake cycle—To investigate how VTA *Vglut2* neurons influence the sleep-wake cycle over 24 hours, we genetically ablated VTA *Vglut2* neurons using AAV-DIO-CASP3 to produce VTA *Vglut2*-CASP3 mice (Fig. 2a, Supplementary Fig. 3d). About 80% of the VTA *Vglut2* neurons were destroyed (Supplementary Fig. 3d). Chronic lesioning of VTA *Vglut2* cells reduced wakefulness, and increased NREM sleep, but only during the “lights off” phase (Fig. 2b). Looking at the sleep-wake microarchitecture, wake consolidation was impaired, with more episodes and shorter episode durations of wake (Fig. 2c), and with more transitions between wake and NREM sleep (Fig. 2d), again with the phenotype appearing selectively during lights off”.

VTA *Vglut2* neurons are selectively wake- and REM sleep-active—To determine when during the natural sleep-wake cycle the VTA *Vglut2* neurons were active, we made VTA *Vglut2*-GCaMP6 mice (Fig. 2e), then recorded Ca²⁺ signals by fiber photometry (Fig. 2f; Supplementary Fig. 3e). (Note: we used GCaMP6s for all this and all subsequent photometry experiments). The Ca²⁺ signal increased selectively during wakefulness and REM sleep (Fig. 2f, g), and with novel objects and female scents (Supplementary Fig. 3e). During NREM sleep, the VTA *Vglut2* neurons had lower Ca²⁺ signals (Fig. 2f, g). At the transitions between the vigilance states, the F/F ratio increased from NREM to wake and from NREM to REM sleep (Fig. 2h), but decreased from wakefulness to NREM. The F/F ratio changed little from REM sleep to wake transitions (Fig. 2h). [As controls, no changes in the F/F ratio were found by photometry between vigilance states in VTA *Vglut2*-GFP mice (Supplementary Fig. 3f, g); furthermore, there was no bleaching of the signal in VTA *Vglut2*-GCaMP6s mice, as the F/F ratios stayed constant over 6 hours (Supplementary Fig. 3h)].

VTA *Vglut2* neurons promote wakefulness independently of dopamine

Dopamine neurons in the VTA promote wakefulness^{5,8}, so we tested if the wake-promoting effect of VTA *Vglut2* neurons depended on dopamine. We first verified that VTA *Vglut2* neurons are largely distinct from VTA dopamine neurons. Immunohistochemistry confirmed that only 26 ± 1.6% of the *Vglut2* cells were TH-positive (Supplementary Fig. 4a, b), as shown previously²⁴. Unlike dopamine neurons, VTA *Vglut2* cells were mostly located in the midline VTA nuclei - the rostral linear nucleus (RLi) and the interfascicular nucleus (IF) (Supplementary Fig. 4b)^{24,34}. Thus, the majority of VTA *Vglut2* and VTA^{DA} neurons are distinct populations. We next chemogenetically activated the VTA *Vglut2* neurons in VTA *Vglut2*-hM3Dq mice with CNO in the presence of systemically administered dopamine antagonists SCH-23390 and raclopride for D1 and D2/D3 receptors respectively (Supplementary Fig. 4c, d) (note: mice were injected *i.p.* with the dopamine receptor antagonists 30 mins before CNO *i.p.* injection – please see Methods for drug concentrations). Even when dopamine receptors were blocked, VTA *Vglut2* neurons still promoted wakefulness (Supplementary Fig. 4d).

VTA *Vglut2* neurons promote wakefulness via the nucleus accumbens and the lateral hypothalamus

To identify the brain areas that participate in generating the VTA *Vglut2*-mediated wakefulness, we mapped cFOS activity in VTA *Vglut2*-hM3Dq mice. Following CNO *i.p.* injection, increased numbers of cFOS-positive cells were identified in multiple brain regions (Fig. 3a and Supplementary Fig. 5a, b). cFOS expression was particularly activated in the lateral hypothalamus (LH), nucleus accumbens (NAc) and ventral pallidum (VP) (Fig. 3a and Supplementary Fig. 5a, b). In the LH, 60% of cFOS-expressing cells that were activated by CNO *i.p.* injections were also orexin-positive compared with the low number of cFOS expressing cells following saline injection (Supplementary Fig. 5c).

We then undertook ChR2-based circuit mapping of the VTA *Vglut2* neurons in VTA *Vglut2*-ChR2-EYFP mice (Fig. 3b, Supplementary Fig. 5d). Consistent with the cFOS activation data, there was a dense projection of VTA *Vglut2* neurons to the LH and NAc (Fig. 3b and

Supplementary Fig. 5c), as described previously^{29,30,35,36}. To test whether the VTA $Vglut2 \rightarrow$ LH or VTA $Vglut2 \rightarrow$ NAc projections can promote wakefulness, we placed optical fibers into the LH and NAc of VTA $Vglut2$ -Chr2-EYFP mice to stimulate the terminals (Fig. 3c, d, e, f). Optically stimulating VTA $Vglut2$ fibers in the LH strongly and consistently promoted waking from NREM sleep (Fig. 3c; Supplementary Fig. 6a); and chronic optical stimulation for 3 hours maintained wakefulness (Fig. 3d). Similarly, optogenetic stimulation of the VTA $Vglut2$ terminals in the NAc promoted waking from NREM sleep (Fig. 3e; Supplementary Fig. 6b) and chronic optogenetic stimulation for 3 hours increased wakefulness and reduced NREM and REM sleep (Fig. 3f). Thus the LH and NAc are two areas contributing to wakefulness when excited by VTA $Vglut2$ neurons.

Nitric oxide synthase marks wake-promoting VTA $Vglut2$ neurons—To confirm the wake-promoting actions of the VTA $Vglut2 \rightarrow$ LH and VTA $Vglut2 \rightarrow$ NAc projections, we used retrograde-labeling by injecting AAV-Retro-DIO-Chronos-GFP into the LH and NAc of $Vglut2$ -ires-Cre mice. We identified many GFP-positive soma in the VTA (Supplementary Fig. 7a, b). We optogenetically activated the Chronos-GFP retrolabeled cells by inserting optical fibers into the VTA (Supplementary Fig. 7b). Tonic opto-activation increased cFOS in these retro-labeled neurons (control: 31 ± 5 , stimulation: 206 ± 41) (Supplementary Fig. 7c). Activation of the retro-labeled NAc \rightarrow VTA $Vglut2$ neurons increased wakefulness (Supplementary Fig. 7d). To profile these retro-labeled VTA $Vglut2$ neurons, we stained VTA $Vglut2$ neurons with a panel of antibodies recognizing neurochemical markers (nitric oxide synthase NOS1, tyrosine hydroxylase TH, glutamic acid decarboxylase GAD67, parvalbumin PV, somatostatin SOM) (Fig. 4a, Supplementary Fig. 7e). Of these markers, double-labelling of retrolabeled NAc \rightarrow VTA $Vglut2$ and LH \rightarrow VTA $Vglut2$ neurons identified that about $68 \pm 9\%$ of the GFP-positive cells were immuno-positive for NOS1 (Fig. 4a, Supplementary Fig. 7f), mostly in the midline VTA. This was confirmed by direct double-labelling with VTA $Vglut2$ -Chr2-EYFP neurons and VTA $Nos1$ neurons (Supplementary Fig. 8a, b). About $75 \pm 3\%$ of VTA $Nos1$ cells were VTA $Vglut2$ -positive (Supplementary Fig. 8b), as also seen independently³⁴.

To test if the VTA $Nos1$ neurons are functionally the same as the VTA $Vglut2$ neurons in producing wakefulness, we chemogenetically activated the VTA $Nos1$ neurons by delivering AAV-DIO-hM3Dq-mCherry into the VTA of $Nos1$ -ires-Cre mice (Fig. 4b, c). As for the VTA $Vglut2$ -hM3Dq mice, giving 1 mg/kg CNO *i.p.* to the VTA $Nos1$ -hM3Dq mice produced sustained wakefulness (100%) for 4 hours (Fig. 4c, Supplementary Fig. 8c). Also similar to the VTA $Vglut2$ -hM3Dq mice, the wakefulness produced by *i.p.* administered CNO activation of VTA $Nos1$ neurons was not blocked by systemic *i.p.* administered dopamine D1 and D2/D3 receptor antagonists (Supplementary Fig. 8d) (note: mice were injected *i.p.* with the dopamine receptor antagonists 30 mins before CNO *i.p.* injection – see Methods for drug concentrations). Thus, the wake-promoting VTA $Nos1$ neurons are a subset of VTA $Vglut2$ neurons. Chemogenetic inhibition of these VTA $Vglut2/Nos1$ neurons, by delivering AAV-DIO-hM4Di-mCherry into the VTA of $Nos1$ -ires-Cre mice and giving CNO *i.p.*, decreased wakefulness and produced more NREM sleep (Fig. 4b, Fig. 4d, Supplementary Fig. 8e). Therefore, VTA $Vglut2/Nos1$ neurons can bidirectionally regulate wakefulness. We next mapped projections of VTA $Nos1$ neurons by injecting AAV-DIO-Chr2-EYFP into the VTA

of *Nos1-ires-Cre* mice. Similar to VTA *Vglut2* neurons, VTA *Nos1* neurons project to the NAc, VP and LH (Supplementary Fig. 8f), again implying that the NOS1-expressing neurons are a subset of the glutamatergic ones.

VTA *Vgat* neurons limit wakefulness and induce NREM sleep—We next looked for neurons in the VTA that could potentially restrain the wake-promoting activity of the VTA *Vglut2/Nos1* neurons. The VTA contains many GABAergic neurons (Supplementary Fig. 9a, b)^{24,30}. These can be detected by expression of the vesicular GABA transporter (VGAT). We first confirmed that *Vgat* gene-expressing neurons were mostly distinct from dopamine or glutamate neurons: only $0.3 \pm 0.1\%$ of these GABAergic neurons (as defined by VTA *Vgat*-ChR2-EYFP staining) stained with TH (Supplementary Fig. 9a), and $12 \pm 0.6\%$ of these VTA *Vgat* neurons were NOS1-positive; however, these cells were not in the midline but mostly in the lateral part of the VTA (PBP), which are distinct from VTA *Nos1/Vglut2* populations in the midline (Supplementary Fig. 9b)³⁴.

To examine if VTA *Vgat* neurons contribute to sleep-wake regulation, AAV-DIO-hM3Dq-mCherry or AAV-DIO-hM4Di-mCherry was injected into the VTA of *Vgat-ires-Cre* mice to generate VTA *Vgat*-hM3Dq and VTA *Vgat*-hM4Di mice respectively (Fig. 5a, Supplementary Fig. 9c, d). CNO injection *i.p.* into VTA *Vgat*-hM3Dq mice produced sustained (80%) NREM sleep for 6 hours (Fig. 5b), with continuous δ power in the EEG. Following CNO administration *i.p.*, the latency to NREM sleep was reduced to about 10 minutes compared with saline administration (Fig. 5c). However, latency to REM sleep was significantly increased - there was no REM sleep in the first 6 hours (Fig. 5c) [note: we did several further controls for the specificity of CNO's actions to ensure it was not acting as a sedative after conversion to clozapine³⁷. We injected 1 mg/kg CNO *i.p.* into both AAV-naïve *Vgat-ires-Cre* mice - *i.e.* mice that had not received any AAV injections (Supplementary Fig. 1b), and into VTA *Vgat*-mCherry mice (produced by injecting AAV-DIO-mCherry into the VTA of *Vgat-ires-Cre* mice). In neither of these types of mice did CNO alter the amounts of sleep or wakefulness compared with saline-injected controls, (Supplementary Fig. 1d). In a separate study²¹, we similarly found that CNO systemically injected *i.p.* at the higher concentration of 5 mg/kg into AAV-naïve *Vgat-ires-Cre* mice also did not induce NREM sleep above the background of sleep occurring following saline injection²¹].

In converse experiments with chemogenetic inhibition of VTA *Vgat* neurons, injecting CNO *i.p.* into VTA *Vgat*-hM4Di mice produced 100% wakefulness for 6 hours with sustained theta frequencies in the EEG (Fig. 5d). There was an increased latency to the first NREM and REM sleep bouts to over 6 hours post-injection of CNO *i.p.* compared with saline *i.p.*-injected mice (Fig. 5e).

We next examined if subtypes of GABAergic neuron can induce NREM sleep. Subtypes of GABAergic neurons in the VTA include those expressing parvalbumin (*Pv*), somatostatin (*Som*), and in the PBP region, *Nos1/Vgat*³⁴ (see also Supplementary Fig. 9b). We chemogenetically activated VTA *Pv*, VTA *Som* and VTA-PBP *Nos1/Vgat* populations in the VTA (Supplementary Fig. 10) by expressing hM3Dq-mCherry in these cells. Activation of VTA *Pv* and VTA *Som* neurons each produced 3 hours of NREM sleep (Supplementary Fig. 10). However, activating VTA-PBP *Nos1/Vgat* neurons did not induce either sleep or wakefulness

(Supplementary Fig. 10). Thus, several GABAergic subtypes in the VTA can contribute to induction of NREM sleep, although each group activated individually does not give the full effect obtained with activating VTA *Vgat* neurons.

Lesioning of VTA *Vgat* neurons produces continuous wakefulness—To look at VTA *Vgat* function in the sleep-wake cycle over 24 hours, we chronically lesioned VTA *Vgat* neurons with AAV-DIO-CASP3 (Fig. 6a, Supplementary Fig. 11a). About 88% of the VTA *Vgat* neurons were destroyed (Supplementary Fig. 11a). In these VTA *Vgat*-CASP3 mice, there was an increase in wakefulness in both the “lights on” and “lights off” periods, but especially during the “lights off” period – the VTA *Vgat*-CASP3 animals slept for only 40 minutes, whereas non-lesioned VTA *Vgat*-GFP control mice slept 4 hours in the 12 hours of the “lights off” period (Fig. 6b). During “lights on”, the least active period of the mice, the control mice slept for about 7 hours, and the VTA *Vgat*-CASP3 mice slept for about 6 hours (Fig. 6b). During “lights-off” the average NREM episode duration of VTA *Vgat*-CASP3 mice was much shorter, and transitions between vigilance states were dramatically decreased (Fig. 6c, d). The reduced sleep phenotype of VTA *Vgat*-CASP3 persisted unchanged for at least 4 months, resulting in the mice having a permanent and substantial sleep deficit (Supplementary Fig. 11b).

VTA *Vgat* neurons are selectively wake- and REM-active—Based on the chemogenetic and lesioning results, we might have expected VTA *Vgat* neurons to be NREM sleep-active. To test this, we made VTA *Vgat*-GCaMP6 mice and measured the activity of VTA *Vgat* neurons by fiber photometry during different vigilance states of freely moving mice (Fig. 6e). Surprisingly, as for the *Vglut2* neurons, we found that the Ca²⁺ signal for the VTA *Vgat* neurons actually increased selectively during wakefulness and REM sleep (Fig. 6f). During NREM sleep the VTA *Vgat* cells had a lower Ca²⁺ signal (Fig. 6f, g). At the transitions between the vigilance states (Fig. 6h), the F/F ratio decreased from wakefulness to NREM sleep, and increased from NREM sleep to wake, and from NREM to REM sleep (Fig. 6h). Within an individual bout of wake or REM sleep, the Ca²⁺ signal of the VTA *Vgat* cells did not differ between the earlier and later parts of the bouts (Supplementary Fig. 11c).

To search for NREM sleep-active VTA *Vgat* neurons that might have been missed by fiber photometry, we used micro-endoscopic calcium imaging of these neurons in VTA *Vgat*-GCaMP6f mice (Supplementary Fig. 12). We placed a gradient refractive index (GRIN) lens above the VTA, and recorded fluorescence of VTA *Vgat* neurons during NREM sleep or wakefulness of freely moving mice (Supplementary Fig. 12a). For the single cells that were tracked (16 cells from 4 mice), Ca²⁺ levels in VTA *Vgat* neurons increased during wake and decreased during NREM sleep (Supplementary Fig. 12b, c, d, e, f). This result further confirmed that VTA *Vgat* neurons are selectively wake-active.

VTA *Vgat* neurons reduce wakefulness and induce NREM sleep by both local inhibition and via projections to the LH—Because VTA *Vgat* neurons are selectively wake- and REM-on, we hypothesized that they are not physiologically triggering NREM sleep, but they are instead limiting wakefulness. To explore how VTA *Vgat* neurons do this, we conducted ChR2-based mapping of the projections of VTA *Vgat* axons by delivering AAV-DIO-ChR2-EYFP into the VTA area of *Vgat-ires-Cre* mice. As published previously³⁸,

dense VTA $Vgat$ ChR-positive fibers were found locally in the VTA (Fig. 7a), but also in the LH area (Fig. 7a), and to some extent in the lateral habenula and dentate granule cells of the hippocampus (Supplementary Fig. 13a); a few fibers were also in the PFC and lateral preoptic area (Supplementary Fig. 13a). The especially dense VTA $Vgat$ fibers in the VTA indicate strong local inhibition. To test these connections, we did cFOS activity-mapping by inhibiting VTA $Vgat$ neurons with 1 mg/kg CNO injected *i.p.* into VTA $Vgat$ -hM4D_i mice to examine which areas of the brain expressed cFOS protein (by disinhibition). After CNO injection *i.p.*, which promoted wakefulness (Fig. 5d), cFOS was induced strongly in the VTA and LH (Fig. 7b, Supplementary Fig. 13b, c). Thus, based on cFOS expression as a readout of neuronal excitation, VTA $Vgat$ neurons cause inhibition by projecting to the LH, as well as local inhibition in the VTA.

We confirmed directly that VTA $Vgat$ neurons can mediate local inhibition. We prepared acute brain slices containing the midline VTA from VTA^{Vgat} - $ChR2$ - $EYFP$ mice, optogenetically activated the VTA $Vgat$ neurons (Fig. 7c), and observed the postsynaptic responses in non- $Vgat$ cells. Whole cell patch-clamping confirmed that 87.5% of postsynaptic cells (14 out of 16 cells) received either optogenetically-evoked (o) oIPSCs only, or both oIPSCs and oEPSCs (Fig. 7c); 12.5% of cells (2 out of 16 cells) had oEPSCs only (Fig. 7c). From the relative peak oIPSC and oEPSC ratios, most non- $Vgat$ cells had significantly larger oIPSCs than oEPSCs (Fig. 7c). From single-cell PCR profiling, these non- $Vgat$ neurons with oIPSCs were a mixture of VTA $Vglut2$, VTA^{DA}, and VTA $Vglut2$ /DA neurons (Fig. 7d); the two cells that responded with only oEPSCs were VTA $Vglut2$ and VTA^{DA} cells. Thus, the majority of non- $Vgat$ cells in the midline VTA have a large density of inhibitory input from local VTA $Vgat$ neurons.

Because midline VTA $Vgat$ neurons inhibit midline dopamine neurons, we examined the effect of this local inhibition on wakefulness. We gave D1 and D2/3 receptor antagonists to CNO-injected VTA $Vgat$ -hM4D_i mice (mice were injected *i.p.* with the dopamine receptor antagonists 30 mins before CNO *i.p.* injection – see Methods for drug concentrations). Without dopamine antagonists, CNO inhibition of VTA $Vgat$ neurons caused 6 hours of sustained wakefulness (as shown previously in Fig. 5d). With dopamine receptor antagonists, CNO-induced wakefulness was blocked by 20% (Fig. 7e), implying that the sustained wakefulness originating from the inhibited VTA $Vgat$ neurons could be partially due to the activation (disinhibition) of VTA dopamine neurons.

To test if VTA $Vgat$ neurons use local inhibition to restrict wakefulness, we infused the GABA_A receptor antagonist Gabazine (SR95531) into the VTA of CNO *i.p.*-injected VTA $Vgat$ -hM3Dq mice (please see Methods for Gabazine concentration) (Fig. 7f). In the CNO-injected VTA $Vgat$ -hM3Dq mice, Gabazine reduced CNO-induced NREM sleep by 40% (Fig. 7f). Thus, the sustained NREM sleep originating from the activated VTA $Vgat$ neurons was partially due to local inhibition of VTA $Vglut2$, VTA^{DA}, and VTA $Vglut2$ /DA neurons.

As blocking local GABA transmission with Gabazine did not completely abolish the ability of activated VTA $Vgat$ neurons to induce sustained NREM sleep, the projections of these VTA $Vgat$ neurons might also contribute. We found that following CNO inhibition of

VTA *Vgat* neurons in VTA *Vgat*-hM4Di mice, the number of cFOS-expressing cells in the LH was strongly elevated compared with saline injections (Fig. 7b). About 50% of those FOS-positive LH cells were orexin neurons (Supplementary Fig. 13d). By injecting Retro-AAV-DIO-Chronos-GFP into the LH area of *Vgat-ires-Cre* mice, we also detected dense retro-labeled soma in the VTA (Supplementary Fig. 13e).

The results imply that the VTA *Vgat*→LH projection participates in NREM sleep induction. We therefore placed optical fibers into the LH of VTA *Vgat*-ChR2-EYFP mice to stimulate the terminals of VTA *Vgat* neurons (Fig. 8a). Opto-activating VTA *Vgat* fibers in the LH strongly and consistently initiated wake to NREM sleep transitions (Fig. 8a); Chronic opto-stimulation for 3 hours increased NREM sleep and reduced wakefulness and REM sleep (Fig. 8b). Moreover, activation could also maintain NREM sleep, with much longer episode duration but without affecting REM sleep duration (Fig. 8c), indicating that the VTA *Vgat*→LH projection is sufficient to promote and maintain NREM sleep. However, the EEG power did not differ (Supplementary Fig. 14). Because cFOS expression is highly elevated in the DG when we inhibited VTA *Vgat* neurons (Supplementary Fig. 13c), we also opto-stimulated the VTA *Vgat*→DG projection, but we did not observe any effects on sleep or wakefulness (Supplementary Fig. 15a, b). The above results imply that VTA *Vgat* neurons limit wakefulness by both inhibiting locally VTA glutamatergic and dopaminergic neurons, but also via projection targets (orexin neurons) in the lateral hypothalamus.

Discussion

Our search for novel circuits that promote wakefulness identified wake- and REM sleep-active glutamatergic/NOS1 neurons in the VTA (see Supplementary Fig. 16 for schematic summary). By contrast, we found that VTA GABAergic neurons, when artificially activated, produce a profound sedative state, but surprisingly these neurons, like VTA^{DA} and VTA *Vglut2* cells, are selectively wake- and REM-active during normal sleep⁵. Because of this mismatch between physiological activity and the outcome of artificial activation, we speculate that VTA *Vgat* neurons do not physiologically promote natural NREM sleep, but instead restrain wakefulness. This speculation is, in our view, supported by the results of lesioning the VTA *Vgat* neurons (see below). Alternatively, there could be rare VTA GABAergic neurons, not detected by fiber photometry or *in vivo* Ca²⁺ imaging, that are NREM sleep-active. Such a cell type might actively induce NREM sleep. At the moment there is no direct evidence for either idea, limiting wakefulness or rare NREM-active GABA cells. There are certainly subtypes of GABA neuron in the VTA *e.g.* P_v- and Som-expressing cells, but we found that activating these also induced NREM sleep, although each subtype activated individually does not give the full effect obtained with activating the complete set of VTA *Vgat* neurons. Future work needs to clarify how the subtypes of VTA *Vgat* neurons interact to influence sleep and wakefulness.

When VTA *Vgat* neurons are lesioned this causes permanent sleep loss that persists for months (Supplementary Fig. 11b). It will be interesting to identify metabolic changes produced by this long-term loss of sleep. The effects of the VTA *Vgat* and VTA *Vglut2* lesions, *i.e.* more and less wakefulness respectively, manifest selectively during the “lights-off”/ active phase of the mice (Fig. 2b, Fig. 6a and Supplementary Fig. 11). This fits with

multiunit recordings from mouse VTA neurons, where most cells are under circadian control and fire more during “lights off”³⁹.

Loss of VTA *Vglut2* neurons doubles the number of NREM sleep episodes, and so fragments wakefulness. Nevertheless, the effects of the VTA *Vgat* lesions on wakefulness (Fig. 6a) are greater than those of lesioning VTA *Vglut2* cells (Fig. 2b). It is difficult to predict the effects of ablations. For example, histamine neurons, cholinergic neurons and noradrenergic neurons can be triply lesioned without influencing the baseline amounts of sleep-wake⁴⁰, yet the acute activation or inhibition of these cell groups induces large changes in vigilance state¹. We speculate that VTA *Vgat* neurons are strategically important as they influence diverse targets including VTA *Vglut2*, VTA^{DA} and LH-orexin neurons. Hence the loss of VTA *Vgat* neurons produces large effects. The persistence of this phenotype (chronic wakefulness) post-lesion, suggests no compensation is possible, and perhaps emphasizes the importance of VTA *Vgat* neurons in regulating vigilance state.

We propose that VTA *Vgat* neurons limit wakefulness both via projections to arousal-promoting orexin neurons in the LH (Supplementary Fig. 16), and by inhibiting glutamate and dopamine neurons locally in the VTA. As expected⁴¹, we found some midline VTA *Vgat* neurons co-release glutamate, although the ratio of optically-evoked IPSCs to EPSCs was about 5:1 in favor of inhibition. In the LH, many (60%) of the VTA *Vgat* targets are orexinergic neurons, but VTA *Vgat* terminals could also inhibit wake-promoting GABAergic projection neurons as well^{11,15}.

When VTA *Vgat* neurons are chemogenetically excited the duration of the evoked NREM sleep is remarkable, lasting some 6 hours, similar to sedation. Thus, VTA *Vgat* neurons could, in principle, be a target for novel sedatives that promote a sustained NREM-like sleep (Supplementary Fig. 16). It is surprising that this strong sedative effect arising from activating VTA *Vgat* neurons has not been noticed. Previous work emphasized that activating VTA GABAergic neurons effects motivational states by inhibiting dopamine neurons in the VTA⁴², or by inhibiting cholinergic neurons in the NAc³¹. But in none of these experiments was the EEG recorded, so it is unclear how to interpret the behaviors, especially when decreases in a particular behavior were reported, which could, in fact, be caused by sedation.

Inputs or modulators that physiologically excite VTA *Vgat* neurons will tend to decrease wakefulness. The lateral habenula (LHb) is one such nucleus that sends many excitatory glutamatergic projections to GABAergic neurons in the VTA⁴³. Thus, strong activation of this LHb pathway would be predicted to induce NREM-like sleep. We have found that the anesthetic propofol requires activation of glutamatergic neurons of the lateral habenula to induce sedation *i.e.* slow wave (delta) power in the EEG and motor immobility⁴⁴. Downstream of the LHb, this mechanism could include the activation of the VTA *Vgat* neurons, including those GABAergic cells in the rostromedial tegmental nucleus at the posterior end of the VTA⁴⁵.

As with VTA *Vgat* neurons, the extreme wakefulness produced by stimulating VTA *Vglut2/Nos1* neurons may not have been noticed before because no EEG analysis was performed. We found that the midline VTA *Vglut2/Nos1* neurons promote wakefulness, in part, through the

NAc and in part through the LH. The VTA *Vglut2/Nos1* terminals in the LH could excite GABAergic projection neurons that in turn promote wakefulness^{11,15}, as well as exciting orexin neurons. On the other hand, because lesioning the NAc increases wakefulness^{46,47}, this implies NAc GABAergic projection neurons limit wakefulness, or are actively inducing NREM sleep. If terminals of VTA^{DA} neurons are stimulated in the NAc, wakefulness is produced⁵. This is similar to stimulating the VTA *Vglut2/Nos1* terminals. However, since the wake-promoting effect of VTA *Vglut2/Nos1* neurons is not blocked by dopamine receptor antagonists, it could be that the wake-promoting dopamine terminals do so by promoting glutamate release in the NAc. Similar to our findings, the paraventricular thalamus also promotes wakefulness by sending glutamatergic projections to the NAc¹⁷. It could be that glutamate inputs local GABA neurons in the NAc, which then inhibit the NREM sleep-promoting GABAergic projection neurons. In any case, the NAc is probably a core part of the wake-promoting circuitry.

Similar to GABA and glutamate, NOS1 associates with neurons regulating both wakefulness and sleep^{21,48}. A recent report found *Vglut2/Nos1* projection neurons in the supramammillary nucleus promote wakefulness when chemogenetically activated¹⁴. Our CNO injections to activate mammillary *Vglut2* neurons did not increase wakefulness (Fig. 1j). The reason for the difference is unclear, but in principle there could be a continuous population of *Vglut2/Nos1* cells from the VTA through to the supramammillary nucleus.

What is the significance of the VTA *Vglut2/Nos1* or the VTA *Vgat* neurons being REM active? Activating the VTA *Vglut2/Nos1* or the VTA *Vgat* neurons did not produce REM sleep, and activating VTA *Vgat* neurons during NREM sleep did not alter REM sleep duration (Fig. 8c). Therefore, the VTA *Vglut2* and VTA *Vgat* neurons respond to the primary REM sleep-inducing circuitry, but do not induce or maintain REM sleep.

In summary, our findings on VTA *Vglut2/Nos1* and VTA *Vgat* neurons, and other recent discoveries on dopamine VTA neurons⁵ identify the VTA as a critical center regulating wakefulness. The VTA is exceptionally well-connected, receiving glutamate and GABA inputs from nearly all brain areas^{42,43,49,50}, making it well suited to serve as an integrator of vigilance state. This should be considered when designing experiments to look at the role of the VTA in reward, goal-directed and social behaviours.

Methods

Mice

All experiments were performed in accordance with the UK Home Office Animal Procedures Act (1986); all procedures were approved by the Imperial College Ethical Review Committee and the Ethics Committee for Animal Experimentation of Xijing Hospital, Xi'an, and was conducted according to the Guidelines for Animal Experimentation of Chinese Council institutes. The following strains of mice were used: *Vglut2-ires-Cre: Slc17a6^{tm2(cre)Lowl/J}*, kindly provided by B.B. Lowell, JAX stock 01696351; *Vgat-ires-Cre: Slc32a1^{tm2(cre)Lowl/J}* kindly provided by B.B. Lowell, JAX stock 01696251; *Nos1-ires-Cre^{tm1(cre)Mgmj/J}*, JAX stock 01752652; *Som-ires-Cre: Sst^{tm2.1(cre)Zjh/J}*, JAX stock 01304453; and *Pv-Cre B6; 129P2-Pvalb^{tm1(cre)Arbr/J}*, JAX stock 00806954. All mice used in

the experiments were male and aged 8 weeks at the start of the stereotaxic injections and experiments. Mice were maintained on a 12 hr:12 hr light:dark cycle at constant temp and humidity with ad libitum food and water.

AAV transgene plasmids

pAAV-hSyn-DIO-hM3Dq-mCherry and pAAV-hSyn-DIO-hM4Di-mCherry were gifts from Bryan L. Roth (Addgene plasmids 44361 and 44362)⁵⁵; pAAV-CBA-DIO-GFP was a gift from Edward Boyden (Addgene plasmid 28304); pAAV-EF1 α -DIO-taCASP3-TEV was a gift from Nirao Shah (Addgene plasmid 45580)⁵⁶. pAAV-EF1 α -DIO-hChR2(H314R)-EYFP was a gift from Karl Deisseroth (Addgene plasmid 20298). AAV2/9-CAG-DIO-GCaMP6f was a gift from HanBio Co., Ltd (Shanghai, China), and packaged by BrainVTA (Wuhan, China).

To create pAAV-hSyn-DIO-GCaMP6s, we used the GCaMP6s reading frame from pGP-CMV-GCaMP6s-EGFP (gift of Douglas Kim⁵⁷, Addgene plasmid 40753). The plasmid pAAV-hSyn-DIO-hM3Dq-mCherry (see above) was digested with AscI and NheI, to remove the hM3Dq-mCherry reading frame but keeping both sets of loxP sites to give the pAAV-DIO backbone. The modified GCaMP6s reading frame (in-frame-mutated to remove AscI and NheI sites) was amplified by PCR from pAAV-hsyn-GCaMP6s, digested with AscI and NheI, and then ligated into the pAAV-DIO backbone to give pAAV-hSyn-DIO-GCaMP6s.

Adeno-associated virus (AAV) preparation and stereotaxic injections

To produce AAV (capsid serotype 1/2), the adenovirus helper plasmid *pF 6*, capsid-plasmids pH21 (AAV1) and pRVI (AAV2), and the relevant pAAV transgene plasmid (see section “AAV transgene plasmids”) were co-transfected into HEK293 cells and the subsequent AAV particles were harvested on heparin columns, as described previously^{58,59}.

To produce retro-AAV-DIO-rc(Chronos-GFP), we used the rAAV2 packaging plasmid, a gift from Alla Karpova and David Schaffer⁶⁰ (Addgene plasmid 81070), and the helper plasmid *pF 6*, together with pAAV-EF1 α -DIO-rc[Chronos-GFP], a gift from Edward Boyden⁶¹ (Addgene plasmid 62725). These plasmids were co-transfected into HEK293 cells. To purify the retro-AAV we used the AAVpro Purification Kit (all Serotypes) (Takara-Clontech, Cat#: 6666).

Surgery—Mice were anesthetized 2% isoflurane in oxygen by inhalation and received buprenorphine injection and placed on a stereotaxic frame (Angle Two, Leica Microsystems, Milton Keynes, Buckinghamshire, UK). The AAV was injected through a stainless steel 33-gauge/15mm/PST3 internal cannula (Hamilton) attached to a 10 μ l Hamilton syringe, at a rate of 0.1 μ l min⁻¹.

The injection co-ordinates and volume were (PH/MB)_L: ML (\pm 0.85 mm), AP (-2.7 mm), DV (-5.05 mm), 1.5 μ l + 1.5 μ l;

(PH/MB)_S: ML (\pm 0.85 mm), AP (-2.7 mm), DV (-5.05 mm), 1 μ l + 1 μ l;

LH: ML (\pm 1.00 mm), AP (-1.56 mm), DV (-5.20 mm), 100 nl + 100 nl;

M: ML (± 0.86 mm), AP (-2.7 mm), DV (-5.04 mm), 100 nl + 100 nl;

IPN: ML (-0.02 mm), AP (-3.52 mm), DV (-4.67 mm), 20 nl + 20 nl;

VTA: ML (± 0.35 mm), AP (-3.3 mm), DV (-4.25 mm), 50 nl + 50 nl;

PBP of the VTA: ML (± 0.54 mm), AP (-3.52 mm), DV (-4.29 mm), 20 nl + 20 nl

After injection, the cannula was left at the injection site for at 5 min and then slowly pulled out. After injections, mice were implanted with 3 gold-plated miniature screw electrodes (-1.5 mm Bregma, +1.5 mm midline; +1.5 mm Bregma, -1.5 mm midline; -1 mm Lambda, 0 mm midline – reference electrode) with two EMG wire (AS634, Cooner Wire, CA). The EMG electrodes were inserted between the neck musculature. The EEG-EMG device was affixed to the skull with Orthodontic Resin power and Orthodontic resin liquid (Tocdental, UK).

For the telemetry EEG and EMG surgery, a TL11M2-F20-EET device (Data Science International, USA) was implanted in the abdominal cavity in mice, and four wires of which were subcutaneously lead to mouse's neck by a guiding cannula. Mice were then fixed onto the stereotaxic apparatus in a prone position. A pair of wires was imbedded into the bilateral parietal skulls (AP 0.2 mm, ML 1.5 mm, DV -0.1 mm; AP -1.7 mm, ML -0.2 mm, DV -0.1 mm) by the dental cement to record EEG. The other pair of wires was implanted in the neck muscles to monitor the EMG.

For fiber optogenetic experiments, mice received surgical implantation of a monofiber optic cannula (200 μ m; Doric Lenses, Inc., Quebec, Canada) after virus injection, above the VTA (AP -3.3 mm; ML 0.13 mm; DV -3.93 mm), NAc (AP 1.1 mm; ML 0.6 mm; DV -4.2 mm), DG (AP -1.94 mm; ML 1 mm; DV -2 mm) and LH (AP -1.4 mm; ML 1.0 mm; DV -5.16 mm). For fiber photometry experiments, mice received surgical implantation of a monofiber optic cannula (200 μ m, respectively; Doric Lenses, Inc., Quebec, Canada), after virus injection above the VTA (AP -3.3 mm; ML 0.13 mm; DV -3.93 mm) to target VTA *Vglut2* neurons and (AP -3.3 mm; ML 0.35 mm; DV -4.15 mm) to target VTA *Vgat* neurons and EEG/EMG implants.

The placements of the fibers from all the experiments are shown in Supplementary Fig. 17.

For the microendoscopic calcium imaging, *Vgat-ires-Cre* mice, which had already been injected with AAV2/9-CAG-DIO-GCaMP6f into the VTA were allowed to recovery from surgery for three weeks. They were then re-anesthetized with isoflurane and had TL11M2-F20-EET telemetry devices fitted (see other protocols in the Methods section). The skull was coated with UV curable resin. After 20 s of exposure to ultraviolet light, a protective coating was formed on the skull. A small hole (1 mm diameter) was drilled on the skull (AP -3.45 mm, ML 1.25 mm). To avoid bleeding or drying of the meninges and brain tissue, saline (0.9% NaCl) was superfused constantly. The tissue drill with a PCB bit (500 μ m diameter) was fixed on the stereotaxic frame carefully to remove the brain tissue over the target area. By using a micromanipulator (MP285, Sutter, USA), a GRIN lens (diameter 500 μ m, long 7.6 mm) was slowly implanted into the VTA (AP -3.3 mm, ML 0.35 mm, DV -4.15 mm).

During the insertion process, the lens stayed still for 10 minutes for every 1 mm insertion. The lens was then secured by dental cement and the part left outside the skull was covered by tissue glue (Kwik-Sil). One week later, the tissue glue was removed. The camera (nVista, Inscopix) was connected with the lens to check the fluorescence signals, and then the camera base (baseplate) was secured to the skull with dental cement. After surgery, mice were allowed to recover for at least 2 weeks before experiments. The positions of the GRIN lens placements for all mice are shown in Supplementary Fig. 17f.

Behavioural protocols and drug treatments

For chemogenetic experiments, clozapine-N-oxide (C0832, Sigma-Aldrich, dissolved in saline, 1 mg/kg) or saline was injected *i.p.* and the vigilance states recorded. Mice were split into random groups that received either saline or CNO injection. To test for sleep promoting effects, we injected saline or CNO during the “lights off” period when the mice were likely to be most active; and to test for wake-promoting effects, we injected saline or CNO at the start of the “lights on” period when the mice had their maximum sleep drive. For the PH/MB *Vglut2*-hM3Dq mice, LH *Vglut2*-hM3Dq mice, M *Vglut2*-hM3Dq mice, IPN *Vglut2*-hM3Dq mice, VTA *Vglut2*-hM3Dq mice, VTA *Nos1*-hM3Dq mice, VTA *Vgat*-hM4Di mice, CNO or saline were injected at the start of the “lights on” sleep phase. For the VTA *Nos1*-hM4Di mice, VTA *Vgat*-hM3Dq mice, VTA *Pv*-hM3Dq mice, VTA *Som*-hM3Dq mice, VTA-PBP *Nos1/Vgat*-hM3Dq mice, CNO or saline were injected *i.p.* during the “lights off” active phase. For the optogenetic experiments, VTA *Vglut2*-ChR2-EYFP mice or VTA *Vglut2*-GFP were opto-stimulated (20 Hz, 1 min) during the “lights on” phase; VTA *Vglut2*-ChR2-EYFP→LH or VTA *Vglut2*-ChR2-EYFP→NAc mice were opto-stimulated (20 Hz, 2 min or 5 Hz, 1 min) during the “lights on” sleep phase. For chronic optogenetic stimulation: VTA *Vglut2*-ChR2-EYFP→LH or VTA *Vglut2*-ChR2-EYFP→NAc mice or NAc *Vglut2*-Chronos-GFP→VTA mice were opto-stimulated (20 Hz, 2 s with 58 s interval) at the start of “lights on” sleep phase for 3 hours;

VTA *Vgat*-ChR2-EYFP→LH mice were stimulated (20 Hz, 2 min) during “lights off” active phase. For chronic optogenetic stimulation: VTA *Vgat*-ChR2-EYFP→LH mice were opto-stimulated (20 Hz, 2 s with 58 s interval) at the start of “lights on” sleep phase for 3 hours;

To examine the maintenance of NREM sleep, stimulation were performed during “lights on” sleep phase and EEG/EMG tracing were observed in a real-time window. Laser was turned on for 5 min when NREM sleep occurred.

Note: in all the Ca²⁺ photometry experiments we used GCaMP6s, and for the *in vivo* microscopy experiments for Ca²⁺ imaging we used GCaMP6f. For the photometry experiments, the Ca²⁺ signal of VTA *Vglut2*-GCaMP6 or VTA *Vgat*-GCaMP6 mice were measured for 2 to 6 hours during both the “lights off” wake phase and “lights on” sleep phase. To challenge the mice with novel objects or female, novel objects or female mice were put in the home cage during the “lights off” wake phase and the Ca²⁺ signal of the VTA *Vglut2*-GCaMP6 mice was measured.

For the chemogenetic pharmacological experiments, VTA *Vglut2*-hM3Dq, VTA *Nos1*-hM3Dq or VTA *Vgat*-hM4Di mice were injected (*i.p.*) with dopamine receptor D1 (SCH23390 0.03

mg/kg) and D2/3 receptor antagonists (raclopride 2 mg/kg) injection and 30 min after the antagonists' injection, the mice were received a saline or CNO (1 mg/kg) *i.p.* injection, as previously reported⁸. VTA *Vgat*-hM3Dq mice, gabazine (0.001 μ g) or saline (300 nl) was infused through a gilded cannula according to a previous study⁶². 10 min after infusion, the mice were received saline or CNO (1 mg/kg) by *i.p.* injection.

Locomotor activity—The locomotor activity was detected in an activity test chamber (Med Associates, Inc) with ANY-maze video tracking system. We injected saline or CNO (1 mg/kg) *i.p.* at the start of the “lights on” period when the mice had their maximum sleep drive, and we performed the locomotion experiment 30 min after injection. The behavior was recorded by a video tracking system (ANY-maze) using a camera (FUJIFILM co.) and measured by ANY-maze software (Stoelting Co. US.).

EEG analysis, fiber photometry, microendoscopic calcium imaging, and sleep-wake behavior

EEG and EMG—EEG and EMG signals were recorded using Neurologger 2A devices⁶³ or using TL11M2-F20-EET telemetry devices and dataquest ART (version 4.33). NREM sleep, REM sleep and wake states were first automatically classified using a sleep analysis software Spike2 or NeuroScore and then manually scored.

For the fiber photometry²⁷, a Grass SD9 stimulator was used to control a 473-nm Diode-pumped solid state (DPSS) blue laser with fiber coupler (Shanghai Laser & Optics century Co., Shanghai, China). The laser light was passed through a single source fluorescence cube (FMC_GFP_FC, Doric Lenses, Quebec, Canada) through an optical fiber patch cord (\varnothing 200 μ m, 0.22 NA, Doric Lenses). From the filter cube, a multimodal optical patch cord (\varnothing 200 μ m, 0.37 NA, Doric Lenses) was connected to the mouse chronically implanted fiber (\varnothing 200 μ m, 0.37 NA) with a ceramic split mating sleeves ferrules (Thorlabs, Newton, New Jersey). The GCaMP6 output was then filtered at 500-550 nm using a second dichroic in the fluorescence cube and converted to voltage by an amplified photodiode (APD-FC, Doric Lenses). The photodiode output was amplified by a lock-in amplifier (SR810, Stanford Research Systems, California, USA), also used to drive the laser at 125 Hz with an average power of 80 μ W at the fiber tip. The signal was then digitized using a CED 1401 Micro box (Cambridge Electronic Design, Cambridge, UK) and recorded at 1 kHz using Spike2 software (Cambridge Electronic Design, Cambridge, UK).

Photometry—The photometry signal was matched with the EEG and EMG recordings. For each experiment, the photometry signal F was converted to F/F by $F/F(t)=(F(t)-\text{median}(F))/\text{median}(F)$ ⁵. In some recordings, we observed a decay of photometry signal at the beginning of the recordings. All the sessions were selected after the photometry signal became stable. For the sleep–wake analysis, we performed the recording 3–4 sessions per mouse, each 1–6 hours long and 1 session for 8 hours. To analyze vigilance states for wake, NREM and REM sleep, we selected the all the sessions that mice had all three states⁵, and we calculated the F/F photometry ratio during the contiguous three vigilance states. To analyse the transitions for vigilance states, we selected one randomly chosen session per mouse.

For the micorendoscopic Ca^{2+} imaging⁶⁴, the signal was recorded with the nVista HD system (Inscopix). We analyzed the Ca^{2+} imaging data using ImageJ plug-ins and custom MATLAB script. Video acquisitions were corrected for movement artifacts using TurboReg. Mosaic (Inscopix) was used to analyse the data using independent component analyses (PCA-ICA) as described in previous studies^{65,66}. The $\Delta F/F$ ratio was calculated as $\Delta F/F(t) = (F(t) - \text{median}(F)) / \text{median}(F)$. Ca^{2+} traces and $\Delta F/F$ were matched to the EEG/EMG, which was simultaneously recorded with the Ca^{2+} imaging data.

Immunohistochemistry

Mice were transcardially perfused with 4% paraformaldehyde (Thermo scientific) in phosphate buffered saline (Sigma). Brains were removed and left in 30% sucrose/PBS. 40 or 60- μm -thick coronal sections were cut using a Leica VT1000S vibratome. Free-floating sections were washed in PBS three times for 5 min, permeabilized in PBS plus 0.4% Triton X-100 for 30 min, blocked by incubation in PBS plus 5% normal goat serum (NGS) (Vector), 0.2% Triton X-100 for 1 hour.

Sections were incubated with primary antibody diluted in PBS plus 2% NGS overnight at 4°C in a shaker. Incubated slices were washed three times in PBS for 10 min, and incubated for 2 hours with secondary antibody (Molecular Probes) in PBS and subsequently washed 4 times in PBS for 10 min (all at room temperature).

Primary antibodies used: rabbit polyclonal cFOS (1:4000, Santa Cruz Biotechnology, UK); rat monoclonal mCherry (1:2000, ThermoFisher); rabbit polyclonal GFP (1:1000, ThermoFisher); mouse monoclonal TH (1:2000, Sigma); mouse monoclonal NOS1 (1:200, Santa Cruz, UK); mouse monoclonal NOS1 (1:200, Sigma); rat monoclonal somatostatin (1:1000, Merck); mouse monoclonal parvalbumin (1:1000, Merck); mouse monoclonal Orexin-A (1:200, Santa Cruz, UK). Secondary antibodies were Alexa Fluor 488 goat anti-rabbit, Alexa Fluor 488 goat anti-mouse, Alexa Fluor 594 goat anti-rabbit, Alexa Fluor 594 goat anti-mouse, Alexa Fluor 594 goat anti-rat (1:1000, Invitrogen Molecular Probes, UK).

Slices were mounted on slides, embedded in Mowiol (with DAPI), cover-slipped, and analyzed using an upright fluorescent microscope (Nikon Eclipse 80i, Nikon Corporation, JAPAN) or a Zeiss LSM 510 inverted confocal microscope or a Leica SP5 MP confocal microscope (Facility for Imaging by Light Microscopy, FILM, Imperial College London). Images were acquired using Z-scan.

Acute brain slice electrophysiology and single-cell RT-PCR from the midline VTA area of VTA^{Vgat}-ChR2-EYFP mice

Slice preparation—VTA^{Vgat}-ChR2-EYFP mice were killed by cervical dislocation. Following decapitation, the brains were quickly removed and placed into cold oxygenated N-Methyl-D-glucamine (NMDG) solution (in mM: NMDG 93, HCl 93, KCl 2.5, NaH_2PO_4 1.2, NaHCO_3 30, HEPES 20, glucose 25, sodium ascorbate 5, Thiourea 2, sodium pyruvate 3, MgSO_4 10, CaCl_2 0.5). Coronal brain slices (220- μm thickness) encompassing the midline VTA were obtained using a vibratome (Vibrating Microtome 7000smz-2; Campden Instruments LTD, UK). Slices were kept in NMDG solution at 33°C for 15min with constant

oxygenation, and transferred to fully oxygenated standard aCSF (in mM: NaCl 120, KCl 3.5, NaH₂PO₄ 1.25, NaHCO₃ 25, glucose 10, MgCl₂ 1, CaCl₂ 2) and were maintained in a chamber that was gently and continuously aerated with carbogen gas for at least 90 min at room temperature (20–22 °C) before use for electrophysiology.

Electrophysiological recording from midline VTA neurons innervated by VTA *Vgat* neurons in VTA *Vgat*-ChR2-EYFP mice

Slices were transferred to a submersion recording chamber and were continuously perfused at a rate of 4–5 ml/min with fully oxygenated aCSF at room temperature. For whole-cell recording, patching pipettes at 4–6 MΩ were pulled from autoclaved borosilicate glass capillaries (1.5mm OD, 0.86mm ID, Harvard Apparatus, #GC150F-10) and filled with RNase-free intracellular solution containing (in mM): 140 K-gluconate, 5 NaCl, 10 HEPES, 0.1 EGTA, 2 MgCl₂, 2 Mg-ATP, and 0.3 Na-GTP (pH 7.35, osmolality 285 mOsm) or 125 KCl, 20 NaCl, 10 HEPES, 1 EGTA, 1 CaCl₂, 1 MgCl₂, 2 Mg-ATP and 0.5 Na-GTP (pH 7.35, osmolality 285 mOsm). 0.1% Neurobiotin was included in the intracellular solutions to identify the cell position and morphology following recording. Recordings were performed in current clamp or voltage clamp mode using a Multiclamp 700B amplifier (Molecular Devices, CA). Access and input resistances were monitored throughout the experiments using a 5-mV voltage step. The access resistance was typically <20 MΩ, and results were discarded if resistance changed by more than 20%. Membrane capacitance (C_m) was measured under voltage clamp at -50 mV using a hyperpolarizing 10 mV, 250 ms step. C_m was measured from the change in membrane charge taken from the integrated capacity transients (pClamp, Molecular Devices).

Non YFP+ neurons (presumed non VTA *Vgat* neurons) were visually identified and randomly selected. To maximize RNA recovery, the internal solution in the patch pipette was limited up to 1 μl. A blue light (470 nm) was delivered by TTL-control LED to the entire field through the objective. After the stable voltage clamp was achieved, a single 5 ms or 25 Hz (5 ms) were given at the 30 s and 60 s inter-sweep interval, subsequently. The light intensity was adjusted according to the magnitude of its response.

At the end of each recording, cytoplasm was aspirated into the patch pipette, and expelled into a PCR tube contained lysate buffer. The single cell RT-PCR assays were performed using the Single-Cell to-CT Kit (Ambion). The content of the neuron was aspirated into the recording pipette and expelled into cell lysis/DNase I solution. Reverse transcription and cDNA pre-amplification were performed according to the kit protocol. qPCR was performed using the TaqMan Gene Expression Assay system (Applied Biosystems machine, Foster City, USA). The mouse TaqMan assay probes were designed by, and purchased from Invitrogen (ThermoFisher): m18srRNA, Mm03928990_g1; mSlc17a6 (*Vglut2*) Mm00499876_m1; mSlc6a3 (*dat*) Mm00438388_m1; mTh Mm00447557_m1; mGad1: Mm04207432_g1; mSlc32a1 (*Vgat*) Mm00494138_m1; The single cell gene expression matrix was made in Origin.

Quantification and statistics—All statistical tests were run in “Origin 2015” (Origin Lab). The individual tests we used are given in the figure legends and the details are supplied

in Supplementary Table 1. All data are given as mean \pm SEM unless otherwise stated in the figure legends. No statistical methods were used to pre-determine sample sizes but our sample sizes are similar to those reported in previous publications^{21,44}. The data met the assumptions of the statistical tests used. Before using any given statistical test we formally tested for normality and equal variances. When we found the data were non-normal we used non-parametric tests (details in the relevant figure legends and in Supplementary Table 1). All t-tests were two-sided.

We excluded mice where it was subsequently found that the placement of the opto-fibers was misplaced or that there was no AAV transgene expression or when this expression was in the wrong place. Mice were assigned randomly to the experimental and control groups. When possible, experimental treatments were also randomized. When mice were given drugs versus saline, for example, they received the drug or saline in random order. All experimental data analysis was blinded, including cFOS counting, the analysis of EEG data and animal behaviour that was scored from videos.

Supplementary Material

Refer to Web version on PubMed Central for supplementary material.

Acknowledgements

We thank M. Ungless (Faculty of Medicine, Imperial College London) for comments on the manuscript. Our work was supported by the Wellcome Trust (107839/Z/15/Z, N.P.F. and 107841/Z/15/Z, W.W.); the UK Dementia Research Institute (WW and NPF), and the Funds for International Cooperation and Exchange of the National Natural Science Foundation of China (Grant No. 81620108012, H.D. and N.P.F.); the China Scholarship Council (YM), a Rubicon Fellowship (019.161LW.010) from the Netherlands Organization for Scientific Research (WB), an Imperial College Schrödinger Scholarship (G.M.), and an Imperial College Junior Research Fellowship (JJH). DB and JJH were also supported by The Francis Crick Institute, which receives its core funding from Cancer Research UK (FC001055), the Medical Research Council (FC001055), and the Wellcome Trust (FC001055). The Facility for Imaging by Light Microscopy (FILM) at Imperial College London is in part supported by funding from the Wellcome Trust (grant 104931/Z/14/Z) and BBSRC (grant BB/L015129/1).

References

1. Scammell TE, Arrigoni E, Lipton JO. Neural Circuitry of Wakefulness and Sleep. *Neuron*. 2017; 93:747–765. DOI: 10.1016/j.neuron.2017.01.014 [PubMed: 28231463]
2. Weber F, Dan Y. Circuit-based interrogation of sleep control. *Nature*. 2016; 538:51–59. DOI: 10.1038/nature19773 [PubMed: 27708309]
3. Saper CB, Fuller PM. Wake-sleep circuitry: an overview. *Curr Opin Neurobiol*. 2017; 44:186–192. DOI: 10.1016/j.conb.2017.03.021 [PubMed: 28577468]
4. Gent TC, Bassetti C, Adamantidis AR. Sleep-wake control and the thalamus. *Curr Opin Neurobiol*. 2018; 52:188–197. DOI: 10.1016/j.conb.2018.08.002 [PubMed: 30144746]
5. Eban-Rothschild A, Rothschild G, Giardino WJ, Jones JR, de Lecea L. VTA dopaminergic neurons regulate ethologically relevant sleep-wake behaviors. *Nat Neurosci*. 2016; 19:1356–1366. DOI: 10.1038/nn.4377 [PubMed: 27595385]
6. Yu X, et al. Wakefulness Is Governed by GABA and Histamine Cotransmission. *Neuron*. 2015; 87:164–178. DOI: 10.1016/j.neuron.2015.06.003 [PubMed: 26094607]
7. Cho JR, et al. Dorsal Raphe Dopamine Neurons Modulate Arousal and Promote Wakefulness by Salient Stimuli. *Neuron*. 2017; 94:1205–1219 e1208. DOI: 10.1016/j.neuron.2017.05.020 [PubMed: 28602690]

8. Oishi Y, et al. Activation of ventral tegmental area dopamine neurons produces wakefulness through dopamine D2-like receptors in mice. *Brain Struct Funct.* 2017; 222:2907–2915. DOI: 10.1007/s00429-017-1365-7 [PubMed: 28124114]
9. Kosse C, Schone C, Bracey E, Burdakov D. Orexin-driven GAD65 network of the lateral hypothalamus sets physical activity in mice. *Proc Natl Acad Sci U S A.* 2017; 114:4525–4530. DOI: 10.1073/pnas.1619700114 [PubMed: 28396414]
10. Schone C, Apergis-Schoute J, Sakurai T, Adamantidis A, Burdakov D. Coreleased orexin and glutamate evoke nonredundant spike outputs and computations in histamine neurons. *Cell Rep.* 2014; 7:697–704. DOI: 10.1016/j.celrep.2014.03.055 [PubMed: 24767990]
11. Herrera CG, et al. Hypothalamic feedforward inhibition of thalamocortical network controls arousal and consciousness. *Nat Neurosci.* 2016; 19:290–298. DOI: 10.1038/nn.4209 [PubMed: 26691833]
12. Anacleit C, et al. Basal forebrain control of wakefulness and cortical rhythms. *Nat Commun.* 2015; 6doi: 10.1038/ncomms9744
13. Xu M, et al. Basal forebrain circuit for sleep-wake control. *Nat Neurosci.* 2015; 18:1641–1647. DOI: 10.1038/nn.4143 [PubMed: 26457552]
14. Pedersen NP, et al. Supramammillary glutamate neurons are a key node of the arousal system. *Nat Commun.* 2017; 8doi: 10.1038/s41467-017-01004-6
15. Venner A, Anacleit C, Broadhurst RY, Saper CB, Fuller PM. A Novel Population of Wake-Promoting GABAergic Neurons in the Ventral Lateral Hypothalamus. *Curr Biol.* 2016; 26:2137–2143. DOI: 10.1016/j.cub.2016.05.078 [PubMed: 27426511]
16. Gent TC, Bandarabadi M, Herrera CG, Adamantidis AR. Thalamic dual control of sleep and wakefulness. *Nat Neurosci.* 2018; 21:974–984. DOI: 10.1038/s41593-018-0164-7 [PubMed: 29892048]
17. Ren S, et al. The paraventricular thalamus is a critical thalamic area for wakefulness. *Science.* 2018; 362:429–434. DOI: 10.1126/science.aat2512 [PubMed: 30361367]
18. Weber F, et al. Regulation of REM and Non-REM Sleep by Periaqueductal GABAergic Neurons. *Nat Commun.* 2018; 9doi: 10.1038/s41467-017-02765-w
19. Chung S, et al. Identification of preoptic sleep neurons using retrograde labelling and gene profiling. *Nature.* 2017; 545:477–481. DOI: 10.1038/nature22350 [PubMed: 28514446]
20. Sherin JE, Shiromani PJ, McCarley RW, Saper CB. Activation of ventrolateral preoptic neurons during sleep. *Science.* 1996; 271:216–219. [PubMed: 8539624]
21. Harding EC, et al. A neuronal hub binding sleep initiation and body cooling in response to a warm external stimulus. *Current Biology.* 2018; 28:2263–2273. DOI: 10.1016/j.cub.2018.05.054 [PubMed: 30017485]
22. Anacleit C, et al. The GABAergic parafacial zone is a medullary slow wave sleep-promoting center. *Nat Neurosci.* 2014; 17:1217–1224. DOI: 10.1038/nn.3789 [PubMed: 25129078]
23. Uygun DS, et al. Bottom-Up versus Top-Down Induction of Sleep by Zolpidem Acting on Histaminergic and Neocortex Neurons. *J Neurosci.* 2016; 36:11171–11184. DOI: 10.1523/JNEUROSCI.3714-15.2016 [PubMed: 27807161]
24. Morales M, Margolis EB. Ventral tegmental area: cellular heterogeneity, connectivity and behaviour. *Nat Rev Neurosci.* 2017; 18:73–85. DOI: 10.1038/nrn.2016.165 [PubMed: 28053327]
25. Russo SJ, Nestler EJ. The brain reward circuitry in mood disorders. *Nat Rev Neurosci.* 2013; 14:609–625. DOI: 10.1038/nrn3381 [PubMed: 23942470]
26. Luscher C. The Emergence of a Circuit Model for Addiction. *Annu Rev Neurosci.* 2016; 39:257–276. DOI: 10.1146/annurev-neuro-070815-013920 [PubMed: 27145911]
27. Gunaydin LA, et al. Natural neural projection dynamics underlying social behavior. *Cell.* 2014; 157:1535–1551. DOI: 10.1016/j.cell.2014.05.017 [PubMed: 24949967]
28. Hung LW, et al. Gating of social reward by oxytocin in the ventral tegmental area. *Science.* 2017; 357:1406–1411. DOI: 10.1126/science.aan4994 [PubMed: 28963257]
29. Hnasko TS, Hjelmstad GO, Fields HL, Edwards RH. Ventral tegmental area glutamate neurons: electrophysiological properties and projections. *J Neurosci.* 2012; 32:15076–15085. DOI: 10.1523/JNEUROSCI.3128-12.2012 [PubMed: 23100428]

30. Taylor SR, et al. GABAergic and glutamatergic efferents of the mouse ventral tegmental area. *J Comp Neurol.* 2014; 522:3308–3334. DOI: 10.1002/cne.23603 [PubMed: 24715505]
31. Creed MC, Ntamati NR, Tan KR. VTA GABA neurons modulate specific learning behaviors through the control of dopamine and cholinergic systems. *Front Behav Neurosci.* 2014; 8:8.doi: 10.3389/fnbeh.2014.00008 [PubMed: 24478655]
32. Tan KR, et al. GABA neurons of the VTA drive conditioned place aversion. *Neuron.* 2012; 73:1173–1183. DOI: 10.1016/j.neuron.2012.02.015 [PubMed: 22445344]
33. Taylor NE, et al. Optogenetic activation of dopamine neurons in the ventral tegmental area induces reanimation from general anesthesia. *Proc Natl Acad Sci U S A.* 2016; doi: 10.1073/pnas.1614340113
34. Paul EJ, et al. nNOS-expressing neurons in the ventral tegmental area and substantia nigra pars compacta. *eNeuro.* 2018
35. Qi J, et al. VTA glutamatergic inputs to nucleus accumbens drive aversion by acting on GABAergic interneurons. *Nat Neurosci.* 2016; 19:725–733. DOI: 10.1038/nn.4281 [PubMed: 27019014]
36. Yamaguchi T, Wang HL, Li X, Ng TH, Morales M. Mesocorticolimbic glutamatergic pathway. *J Neurosci.* 2011; 31:8476–8490. DOI: 10.1523/JNEUROSCI.1598-11.2011 [PubMed: 21653852]
37. Gomez JL, et al. Chemogenetics revealed: DREADD occupancy and activation via converted clozapine. *Science.* 2017; 357:503–507. DOI: 10.1126/science.aan2475 [PubMed: 28774929]
38. van Zessen R, Phillips JL, Budygin EA, Stuber GD. Activation of VTA GABA neurons disrupts reward consumption. *Neuron.* 2012; 73:1184–1194. DOI: 10.1016/j.neuron.2012.02.016 [PubMed: 22445345]
39. Fifel K, Meijer JH, Deboer T. Circadian and Homeostatic Modulation of Multi-Unit Activity in Midbrain Dopaminergic Structures. *Sci Rep.* 2018; 8:7765.doi: 10.1038/s41598-018-25770-5 [PubMed: 29773830]
40. Blanco-Centurion C, Gerashchenko D, Shiromani PJ. Effects of saporin-induced lesions of three arousal populations on daily levels of sleep and wake. *J Neurosci.* 2007; 27:14041–14048. DOI: 10.1523/JNEUROSCI.3217-07.2007 [PubMed: 18094243]
41. Root DH, et al. Single rodent mesohabenular axons release glutamate and GABA. *Nat Neurosci.* 2014; 17:1543–1551. DOI: 10.1038/nn.3823 [PubMed: 25242304]
42. Nieh EH, et al. Inhibitory Input from the Lateral Hypothalamus to the Ventral Tegmental Area Disinhibits Dopamine Neurons and Promotes Behavioral Activation. *Neuron.* 2016; 90:1286–1298. DOI: 10.1016/j.neuron.2016.04.035 [PubMed: 27238864]
43. Faget L, et al. Afferent Inputs to Neurotransmitter-Defined Cell Types in the Ventral Tegmental Area. *Cell Rep.* 2016; 15:2796–2808. DOI: 10.1016/j.celrep.2016.05.057 [PubMed: 27292633]
44. Gelegen C, et al. Excitatory Pathways from the Lateral Habenula Enable Propofol-Induced Sedation. *Curr Biol.* 2018; 28:580–587 e585. DOI: 10.1016/j.cub.2017.12.050 [PubMed: 29398217]
45. Zhou TC, Fields HL, Baxter MG, Saper CB, Holland PC. The rostromedial tegmental nucleus (RMTg), a GABAergic afferent to midbrain dopamine neurons, encodes aversive stimuli and inhibits motor responses. *Neuron.* 2009; 61:786–800. DOI: 10.1016/j.neuron.2009.02.001 [PubMed: 19285474]
46. Qiu MH, Vetrivelan R, Fuller PM, Lu J. Basal ganglia control of sleep-wake behavior and cortical activation. *Eur J Neurosci.* 2010; 31:499–507. DOI: 10.1111/j.1460-9568.2009.07062.x [PubMed: 20105243]
47. Qiu MH, et al. The role of nucleus accumbens core/shell in sleep-wake regulation and their involvement in modafinil-induced arousal. *PLoS One.* 2012; 7:e45471.doi: 10.1371/journal.pone.0045471 [PubMed: 23029032]
48. Morairty SR, et al. A role for cortical nNOS/NK1 neurons in coupling homeostatic sleep drive to EEG slow wave activity. *Proc Natl Acad Sci U S A.* 2013; 110:20272–20277. DOI: 10.1073/pnas.1314762110 [PubMed: 24191004]
49. Geisler S, Derst C, Veh RW, Zahm DS. Glutamatergic afferents of the ventral tegmental area in the rat. *J Neurosci.* 2007; 27:5730–5743. DOI: 10.1523/JNEUROSCI.0012-07.2007 [PubMed: 17522317]

50. Beier KT, et al. Circuit Architecture of VTA Dopamine Neurons Revealed by Systematic Input-Output Mapping. *Cell*. 2015; 162:622–634. DOI: 10.1016/j.cell.2015.07.015 [PubMed: 26232228]
51. Vong L, et al. Leptin action on GABAergic neurons prevents obesity and reduces inhibitory tone to POMC neurons. *Neuron*. 2011; 71:142–154. DOI: 10.1016/j.neuron.2011.05.028 [PubMed: 21745644]
52. Leshan RL, Greenwald-Yarnell M, Patterson CM, Gonzalez IE, Myers MG Jr. Leptin action through hypothalamic nitric oxide synthase-1-expressing neurons controls energy balance. *Nat Med*. 2012; 18:820–823. DOI: 10.1038/nm.2724 [PubMed: 22522563]
53. Taniguchi H, et al. A resource of Cre driver lines for genetic targeting of GABAergic neurons in cerebral cortex. *Neuron*. 2011; 71:995–1013. DOI: 10.1016/j.neuron.2011.07.026 [PubMed: 21943598]
54. Hippenmeyer S, et al. A developmental switch in the response of DRG neurons to ETS transcription factor signaling. *PLoS Biol*. 2005; 3:e159.doi: 10.1371/journal.pbio.0030159 [PubMed: 15836427]
55. Krashes MJ, et al. Rapid, reversible activation of AgRP neurons drives feeding behavior in mice. *J Clin Invest*. 2011; 121:1424–1428. DOI: 10.1172/JCI46229 [PubMed: 21364278]
56. Yang CF, et al. Sexually dimorphic neurons in the ventromedial hypothalamus govern mating in both sexes and aggression in males. *Cell*. 2013; 153:896–909. DOI: 10.1016/j.cell.2013.04.017 [PubMed: 23663785]
57. Chen TW, et al. Ultrasensitive fluorescent proteins for imaging neuronal activity. *Nature*. 2013; 499:295–300. DOI: 10.1038/nature12354 [PubMed: 23868258]
58. Klugmann M, et al. AAV-mediated hippocampal expression of short and long Homer 1 proteins differentially affect cognition and seizure activity in adult rats. *Mol Cell Neurosci*. 2005; 28:347–360. DOI: 10.1016/j.mcn.2004.10.002 [PubMed: 15691715]
59. Murray AJ, et al. Parvalbumin-positive CA1 interneurons are required for spatial working but not for reference memory. *Nat Neurosci*. 2011; 14:297–299. DOI: 10.1038/nn.2751 [PubMed: 21278730]
60. Tervo DG, et al. A Designer AAV Variant Permits Efficient Retrograde Access to Projection Neurons. *Neuron*. 2016; 92:372–382. DOI: 10.1016/j.neuron.2016.09.021 [PubMed: 27720486]
61. Klapoetke NC, et al. Independent optical excitation of distinct neural populations. *Nat Methods*. 2014; 11:338–346. DOI: 10.1038/nmeth.2836 [PubMed: 24509633]
62. Jennings JH, et al. Distinct extended amygdala circuits for divergent motivational states. *Nature*. 2013; 496:224–228. DOI: 10.1038/nature12041 [PubMed: 23515155]
63. Anisimov VN, et al. Reconstruction of vocal interactions in a group of small songbirds. *Nat Methods*. 2014; 11:1135–1137. DOI: 10.1038/nmeth.3114 [PubMed: 25262206]
64. Flusberg BA, et al. High-speed, miniaturized fluorescence microscopy in freely moving mice. *Nat Methods*. 2008; 5:935–938. DOI: 10.1038/nmeth.1256 [PubMed: 18836457]
65. Groessl F, et al. Dorsal tegmental dopamine neurons gate associative learning of fear. *Nat Neurosci*. 2018; 21:952–962. DOI: 10.1038/s41593-018-0174-5 [PubMed: 29950668]
66. Chen KS, et al. A Hypothalamic Switch for REM and Non-REM Sleep. *Neuron*. 2018; 97:1168–1176 e1164. DOI: 10.1016/j.neuron.2018.02.005 [PubMed: 29478915]

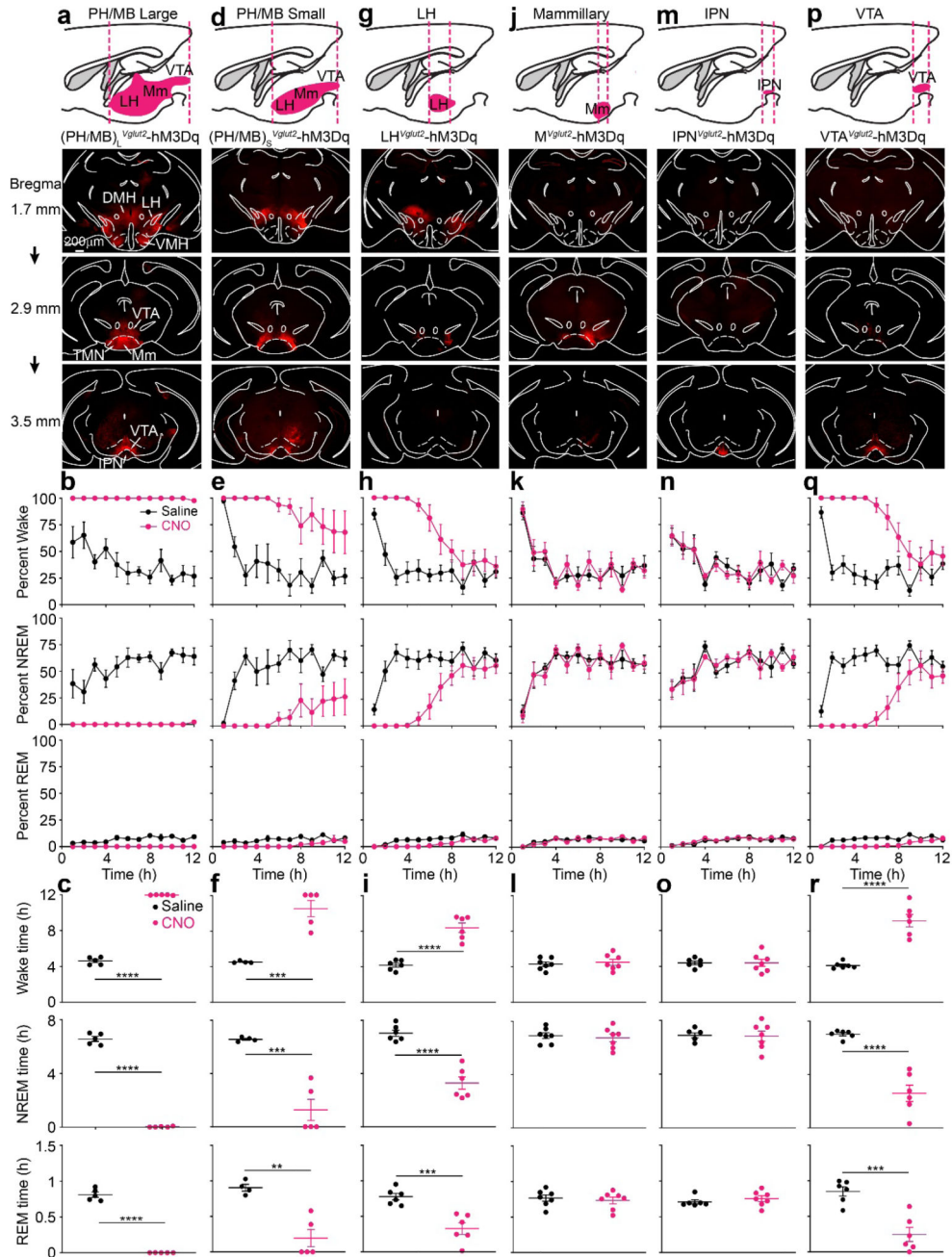


Fig. 1. Chemogenetic mapping for novel glutamatergic areas in the posterior hypothalamus and midbrain that promote wakefulness identifies the VTA

AAV-DIO-hM3Dq-mCherry was injected into different areas of the brain of *Vglut2-ires-Cre* mice. AAV expression was determined by immunocytochemistry for mCherry (red). The images show the actual mCherry staining.

(a, b and c) AAV injection into a large volume of posterior hypothalamus and midbrain (PH/MB)_L. The experiment in (a) was repeated independently 5 times. The graphs show percent of wake, NREM and REM sleep and how these states vary with saline (n=5 mice) or CNO (n=5 mice) *i.p.* injections.

(d, e and f) AAV injection into a smaller volume of posterior hypothalamus and midbrain, and sleep-wake states scored as above after saline (n=4 mice) or CNO (n=5 mice) *i.p.* injections. The experiment in (d) was repeated independently 5 times.

(g, h and i) AAV injection was restricted to the LH, and sleep wake states scored following saline and CNO injection after saline (n=6 mice) or CNO (n=6 mice) *i.p.* injections. The experiment in (g) was repeated independently 6 times.

(j, k and l) AAV injection was restricted to the mammillary area, and sleep wake states scored following saline (n=7 mice) and CNO (n=7 mice) *i.p.* injection. The experiment in (j) was repeated independently 5 times. See Supplementary Fig. 2a for examples of hM3Dq-mCherry expression in individual mice.

(m, n and o) AAV injection was restricted to the interpeduncular nucleus (IPN), and sleep wake states scored following saline (n=6 mice) and CNO (n=7 mice) *i.p.* injection. The experiment in (m) was repeated independently 6 times. See Supplementary Fig. 2b for examples of individual hM3Dq-mCherry expression.

(p, q and r) AAV injection was restricted to the VTA, and sleep wake states scored following saline (n=6) and CNO (n=6) *i.p.* injection. The experiment in (p) was repeated independently 6 times. See Supplementary Fig. 2c for examples of hM3Dq-mCherry expression in individual mice.

DMH, dorsomedial hypothalamus; LH, lateral hypothalamus; PH, posterior hypothalamus; IPN, interpeduncular nucleus; MM, medial mammillary area; TMN, tuberomammillary area; VMH, ventromedial hypothalamus; VTA ventral tegmental area. All error bars represent the SEM. ** $p < 0.01$, *** $p < 0.001$, **** $p < 0.0001$; two-sided unpaired t-test. For detailed statistics information, see Supplementary Table 1.

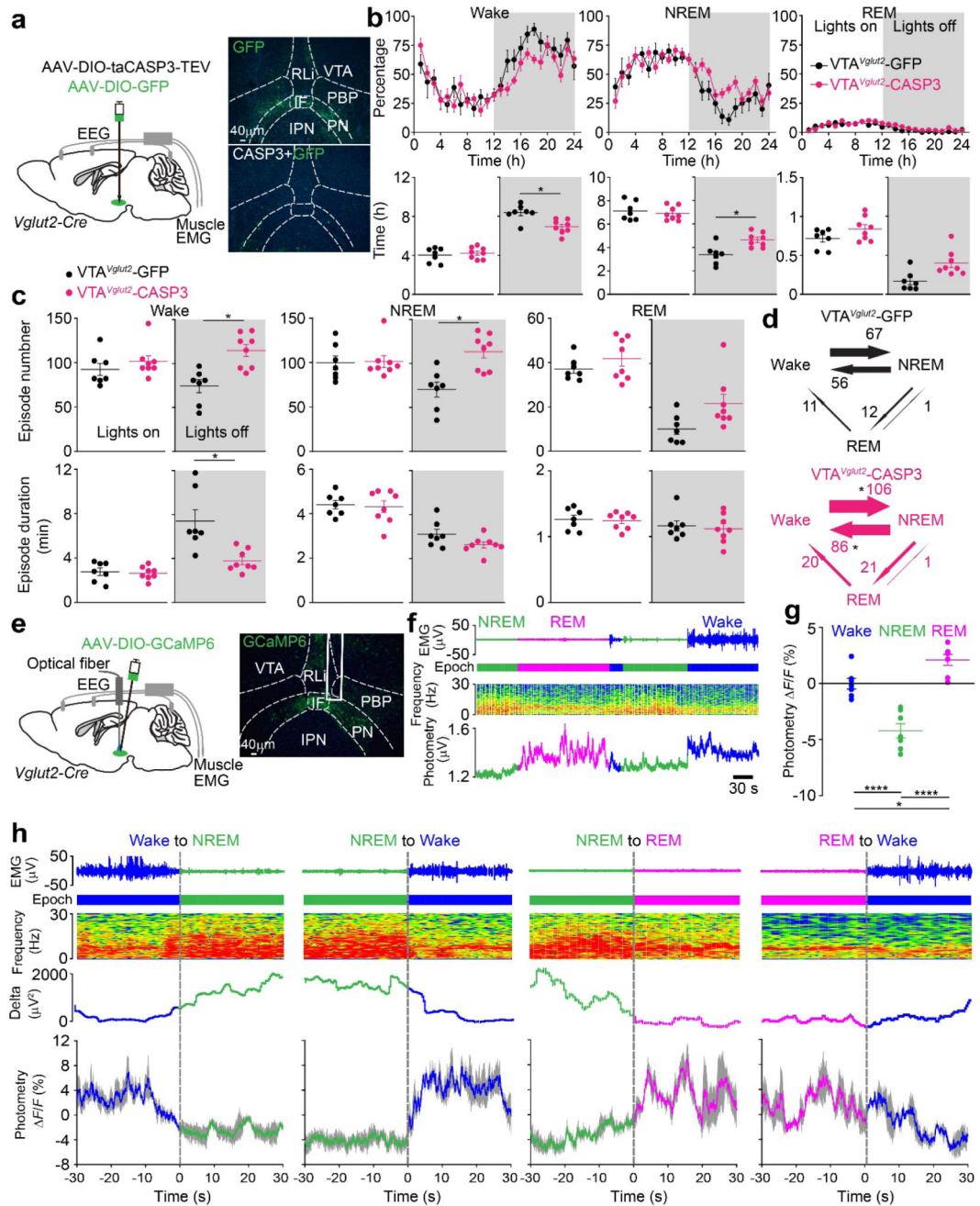


Fig. 2. VTA *Vglut2* neurons consolidate wakefulness and are selectively wake- and REM sleep-active

(a) Lesioning of VTA *Vglut2* neurons. Injection of AAV-DIO-GFP (control) or AAV-DIO-GFP and AAV-DIO-taCASP3-TEV into the VTA area of *Vglut2-ires-Cre* mice. Pictures show GFP control expression in the VTA area of *VTA^{Vglut2}-GFP* mice and that this GFP expression has been greatly diminished in the *VTA^{Vglut2}-CASP3* mice. The experiment was repeated independently 6 times. IF, interfascicular nucleus; IPN, interpeduncular nucleus; PBP, parabrachial pigmented nucleus; PN, paragnigral nucleus; PBP, parabrachial pigmented nucleus; RLi, rostral linear nucleus.

(b) Lesioning of VTA *Vglut2* neurons. Percentage of wake, NREM and REM sleep in control VTA *Vglut2*-GFP mice (n=7 mice) and VTA *Vglut2*-CASP3 mice (n=8 mice), and the total vigilance times in the “lights on” and “lights off” periods.

(c, d) Lesioning of VTA *Vglut2* neurons. Episode number and duration for wake, NREM and REM sleep, and vigilance state transitions during the “lights off” periods in VTA *Vglut2*-GFP control mice (n=7 mice) and VTA *Vglut2*-CASP3 mice (n=8 mice).

(e) Fiber photometry for VTA *Vglut2* neurons. Injection of AAV-DIO-GCaMP6 into the VTA of the *Vglut2-ires-Cre* mice. The experiment was repeated independently 7 times. GCaMP6 expression can be detected in the VTA area and the trace of where the optical fiber was placed is marked.

(f) Fiber photometry Ca^{2+} spectra (bottom trace) recorded in the VTA of VTA *Vglut2*-GCaMP6 mice aligned with the EEG spectra (middle trace) and EMG (top trace) during wakefulness, NREM and REM sleep. “Epoch” indicates vigilance state: blue, wake; green, NREM sleep; magenta, REM sleep.

(g) Fiber photometry F/F ratio of the Ca^{2+} signal in VTA *Vglut2*-GCaMP6 mice during wakefulness, NREM sleep and REM sleep (n=7 mice; 38 sessions).

(h) Detail of how the Ca^{2+} photometry signal in VTA *Vglut2*-GCaMP6 mice changes at the boundaries of the vigilance states (n=7 mice). Ca^{2+} photometry F/F ratio (bottom trace) in the VTA *Vglut2*-GCaMP6 mice aligned with the extracted δ power in the EEG, the EEG spectra itself and EMG during wakefulness, NREM and REM sleep. “Epoch” indicates vigilance state: blue, wake; green, NREM sleep; magenta, REM sleep. Grey shaded regions represent SEM.

* $p < 0.05$, ** $p < 0.01$, **** $p < 0.0001$; For b-d, two-sided unpaired t-test, for g, one-way ANOVA. All error bars represent the SEM. For detailed statistics information, see Supplementary Table1.

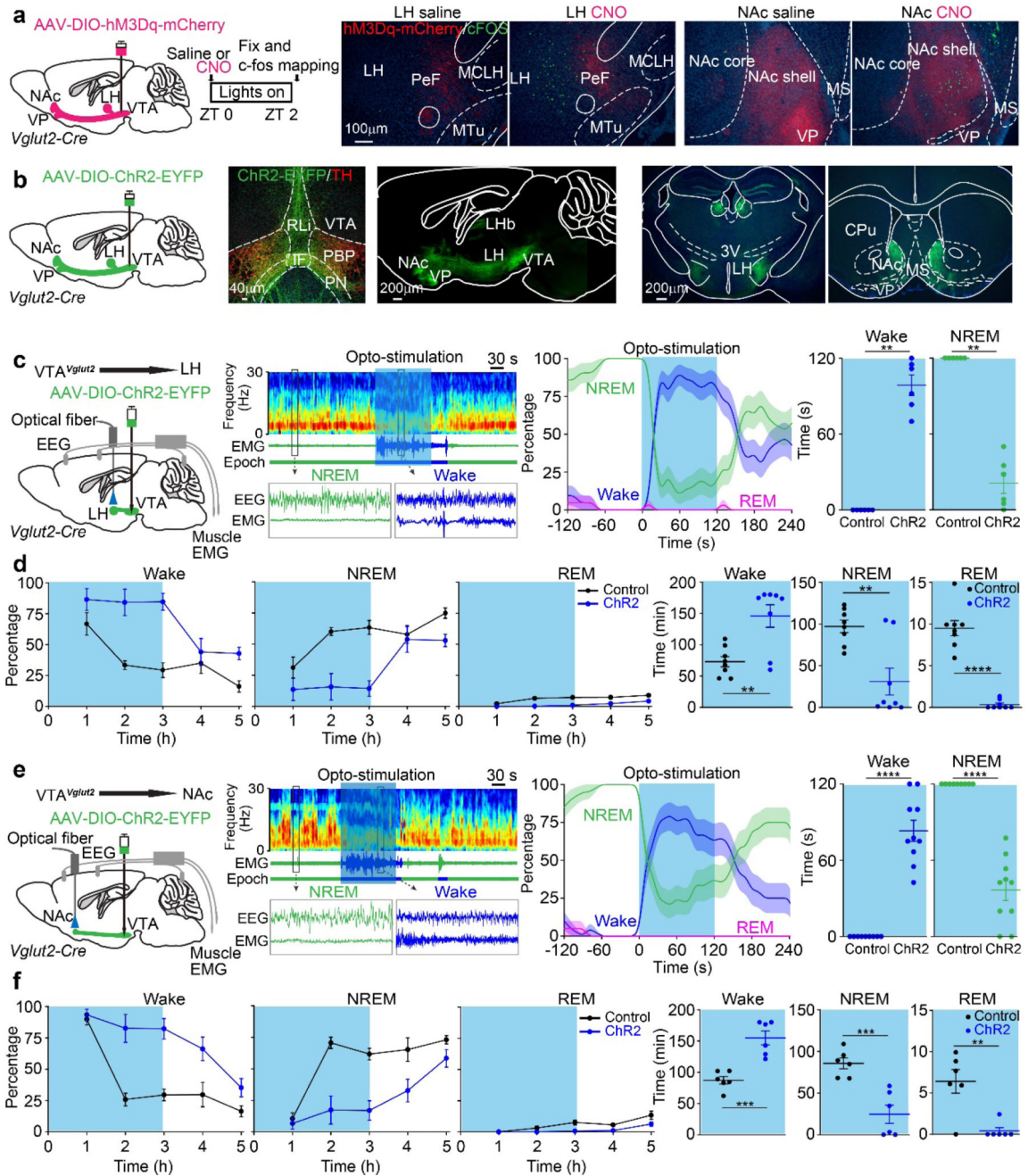


Fig. 3. VTA *Vglut2* neurons promote wakefulness by their projections to the LH and NAC
 (a) cFOS-based activity mapping of brain regions after exciting VTA *Vglut2* neurons. In VTA *Vglut2*-hM3Dq mice, labelled axons mainly project from the VTA to the LH and NAc. cFOS protein expression in neurons of the LH and NAc of VTA *Vglut2*-hM3Dq mice 2 hours after saline or CNO *i.p.* injection at ZT0. The red in the histology figure is the primary fluorescence of the hM3Dq-mCherry-positive axons coming from the VTA area, the cFOS immunohistochemistry is shown in green. The experiment was repeated independently 6 times.

CPu, caudate-putamen; IF, interfascicular nucleus; LH, lateral hypothalamus; LHb, lateral habenula; MS, medial septum; NAc, nucleus accumbens; PeF, perifornical area; PBP, parabrachial pigmented nucleus; PN, paranigral nucleus; PBP, parabrachial pigmented nucleus; RLi, rostral linear nucleus; 3V, third ventricle; VP, ventral pallidum

(b) Axonal projections of VTA *Vglut2* neurons. AAV-DIO-ChR2-EYFP was delivered into the VTA of *Vglut2-ires-Cre* mice, and axons projecting to the LH and NAc were strongly labelled. The experiment was repeated independently 4 times.

(c, d) To functionally investigate the VTA *Vglut2*→LH projection, an optical fiber was placed into the LH area of VTA *Vglut2-ChR2-EYFP* mice. (c) Mice were given 120 s of optostimulation (20 Hz) during NREM sleep (“lights on” period) and the percentage and time of wake and NREM were scored (control: n=6 mice; 23 trials; ChR2: n=6 mice; 21 trials). (d) *VTA Vglut2-ChR2-EYFP* mice (control: n=8 mice; ChR2: n=8 mice) were given 3 hours of opto-stimulation at the start of the sleep period (“lights on” period) and the percentage and time of wake, NREM and REM sleep were scored.

(e, f) To functionally investigate the VTA *Vglut2*→NAc projection, an optical fiber was placed into the NAc area of VTA *Vglut2-ChR2-EYFP* mice. (e) Mice were given 120 s of opto-stimulation (20 Hz) during NREM sleep (“lights on” period) and the percentage and time of wake and NREM were scored (control: n=9 mice; 21 trials; ChR2: n=10 mice; 20 trials). (f) *VTA Vglut2-ChR2-EYFP* mice (control: n=6 mice; ChR2: n=6 mice) were given 3 hours of opto-stimulation at the start of the sleep (“lights on” period) and the percentage and time of wake, NREM and REM sleep were scored.

p<0.01, *p<0.001, ****p<0.0001, for c and e, two-sided mann-whitney u test. For d and f, two-sided unpaired t-test. All error bars represent the SEM. For (c) and (e), the shaded region represents SEM. For detailed statistics information, see Supplementary Table1.

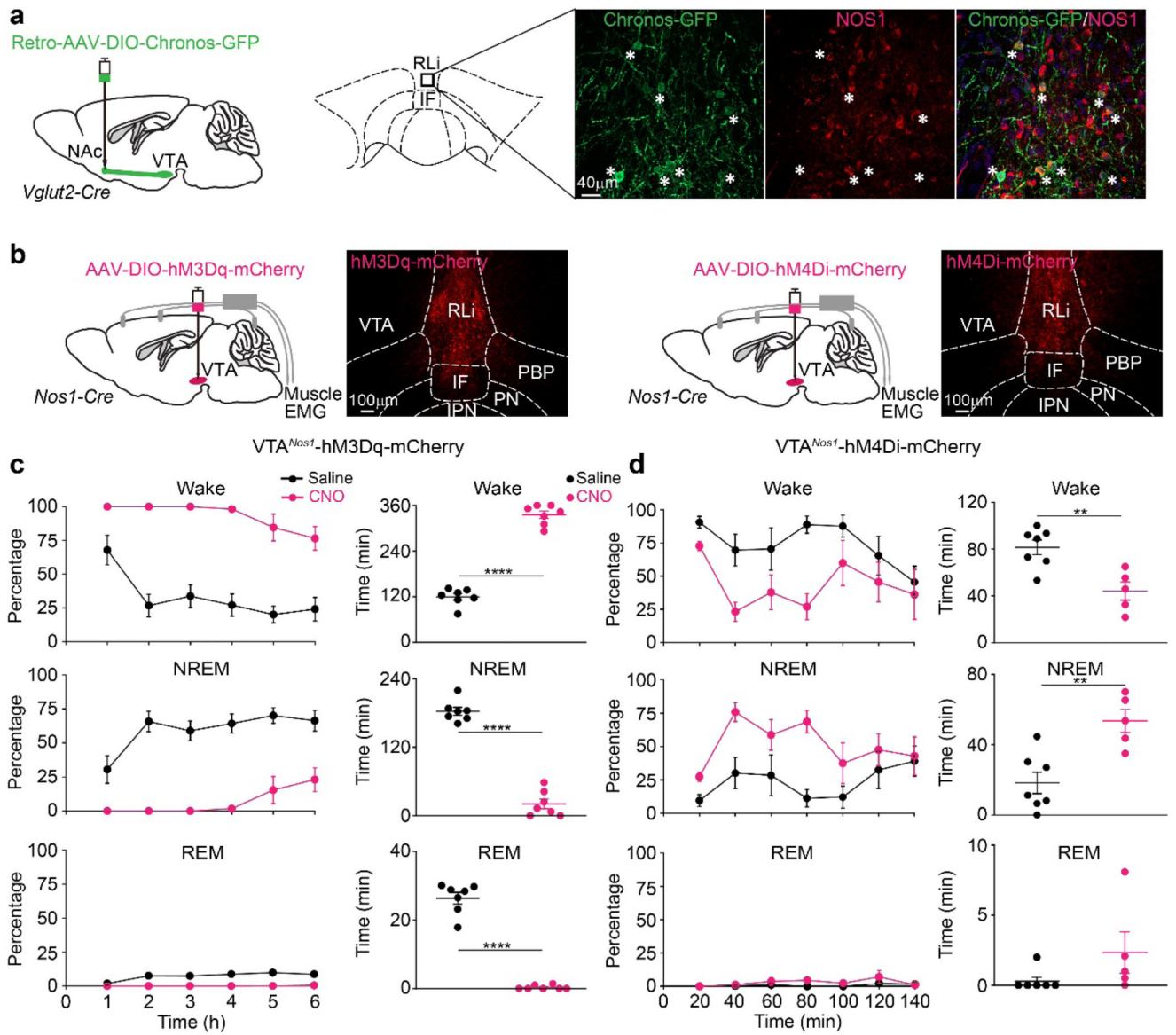


Fig. 4. VTA *Vglut2/Nos1* neurons promote wakefulness

(a) Retro-mapping of VTA *Vglut2*→NAc connections. Retro-AAV-DIO-Chronos-GFP was injected into the NAc of *Vglut2-ires-Cre* mice. Chronos-GFP expression was detected in cells of the VTA and Chronos-GFP retro-labeled VTA midline soma (from the NAc injection) were double-labelled by immunocytochemistry with NOS1 antisera. The experiment was repeated independently 3 times.

(b) Testing how VTA^{Nos1} neurons influence vigilance state. AAV-DIO-hM3Dq-mCherry or AAV-DIO-hM4Di-mCherry was injected into the VTA area of *Nos1-ires-Cre* mice. Images show the expression of hM3Dq-mCherry or hM4Di-mCherry in the VTA. The experiment was repeated independently 6 times.

(c) Excitation of VTA^{Nos1} neurons induces wakefulness. Percentage and time of wake, NREM and REM sleep after saline (n=7 mice) or CNO (n=7 mice) *i.p.* injection at the start of sleep period (“lights on” period) into VTA^{Nos1}-hM3Dq mice.

(d) Inhibition of VTA^{Nos1} neurons induces NREM sleep. Percentage and time of wake, NREM and REM sleep after saline (n=7 mice) or CNO (n=5 mice) *i.p.* injection during wake period (“lights off” period) into VTA^{Nos1}-hM4D_i mice.

IF, interfascicular nucleus; PBP, parabrachial pigmented nucleus; PN, paranigral nucleus; PBP, parabrachial pigmented nucleus; RLi, rostral linear nucleus; VTA, ventral tegmental area

p<0.01, **p<0.0001; two-sided unpaired t-test. All error bars represent the SEM. For detailed statistics information, see Supplementary Table1.

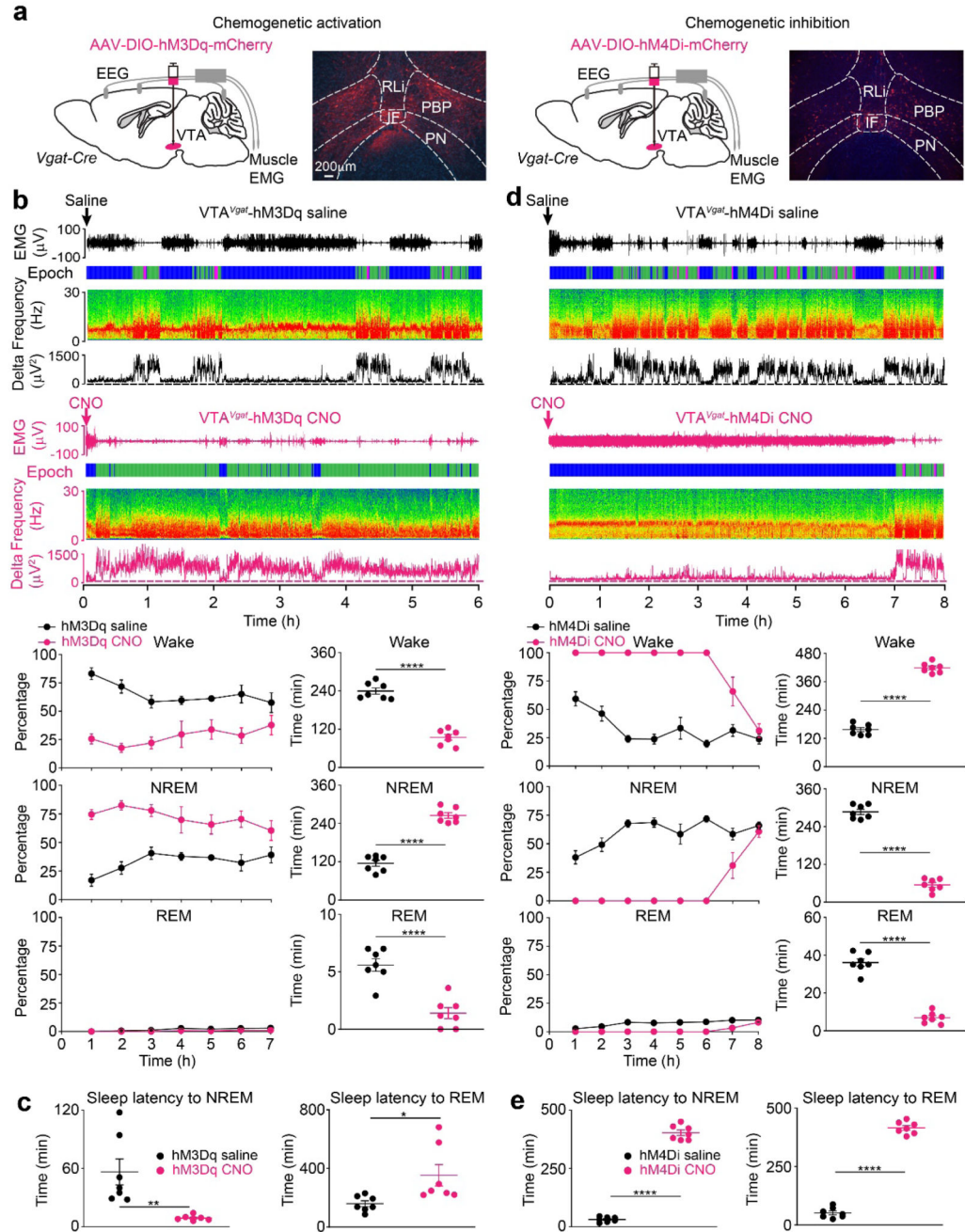


Fig. 5. Excitation of GABAergic neurons in the VTA induces sleep and their inhibition produces continuous wakefulness

(a) Excitation and inhibition of VTA *Vgat* neurons. AAV-DIO-hM3Dq-mCherry or AAV-DIO-hM4Di-mCherry was injected into the VTA of *Vgat-ires-Cre* mice. Images show the expression of hM3Dq-mCherry or hM4Di-mCherry in the VTA. The experiment was repeated independently 6 times. IF, interfascicular nucleus; PBP, parabrachial pigmented nucleus; PN, paragrimal nucleus; PBP, parabrachial pigmented nucleus; RLi, rostral linear nucleus;

- (b) Excitation of VTA V_{gat} neurons induces NREM sleep and suppresses REM sleep. Two individual EEG/EMG spectra and extracted delta power from the EEG are shown for VTA V_{gat} -hM3Dq mice that received saline (n=7 mice) or CNO (n=7 mice) *i.p.* injection during wake period (“lights off” period). The percentage and time in wake, NREM and REM sleep after saline (n=7 mice) or CNO (n=7 mice) injection are shown. “Epoch” indicates vigilance state: blue, wake; green, NREM sleep; magenta, REM sleep.
- (c) Excitation of VTA V_{gat} neurons reduces latency to NREM sleep. Latencies to NREM and REM sleep after saline (n=7 mice) or CNO (n=7 mice) *i.p.* injection into VTA V_{gat} -hM3Dq mice.
- (d) Inhibition of VTA V_{gat} neurons induces wakefulness. Two individual EEG/EMG spectra and extracted delta power from the EEG are shown for VTA V_{gat} -hM4D_i mice that received saline (n=7 mice) or CNO (n=7 mice) *i.p.* injection at the start of sleep period (“lights on” period). The percentage and time in wake, NREM and REM sleep after saline (n=7 mice) or CNO (n=7 mice) *i.p.* injection are shown. “Epoch” indicates vigilance state: blue, wake; green, NREM sleep; magenta, REM sleep.
- (e) Inhibition of VTA V_{gat} neurons increases latency to sleep. Latencies to NREM (n=7 mice) and REM sleep (n=7 mice) after CNO or saline *i.p.* injection into VTA V_{gat} -hM4D_i mice. * $p < 0.05$, ** $p < 0.01$, **** $p < 0.0001$; two-sided unpaired t-test. All error bars represent the SEM. For detailed statistics information, see Supplementary Table1.

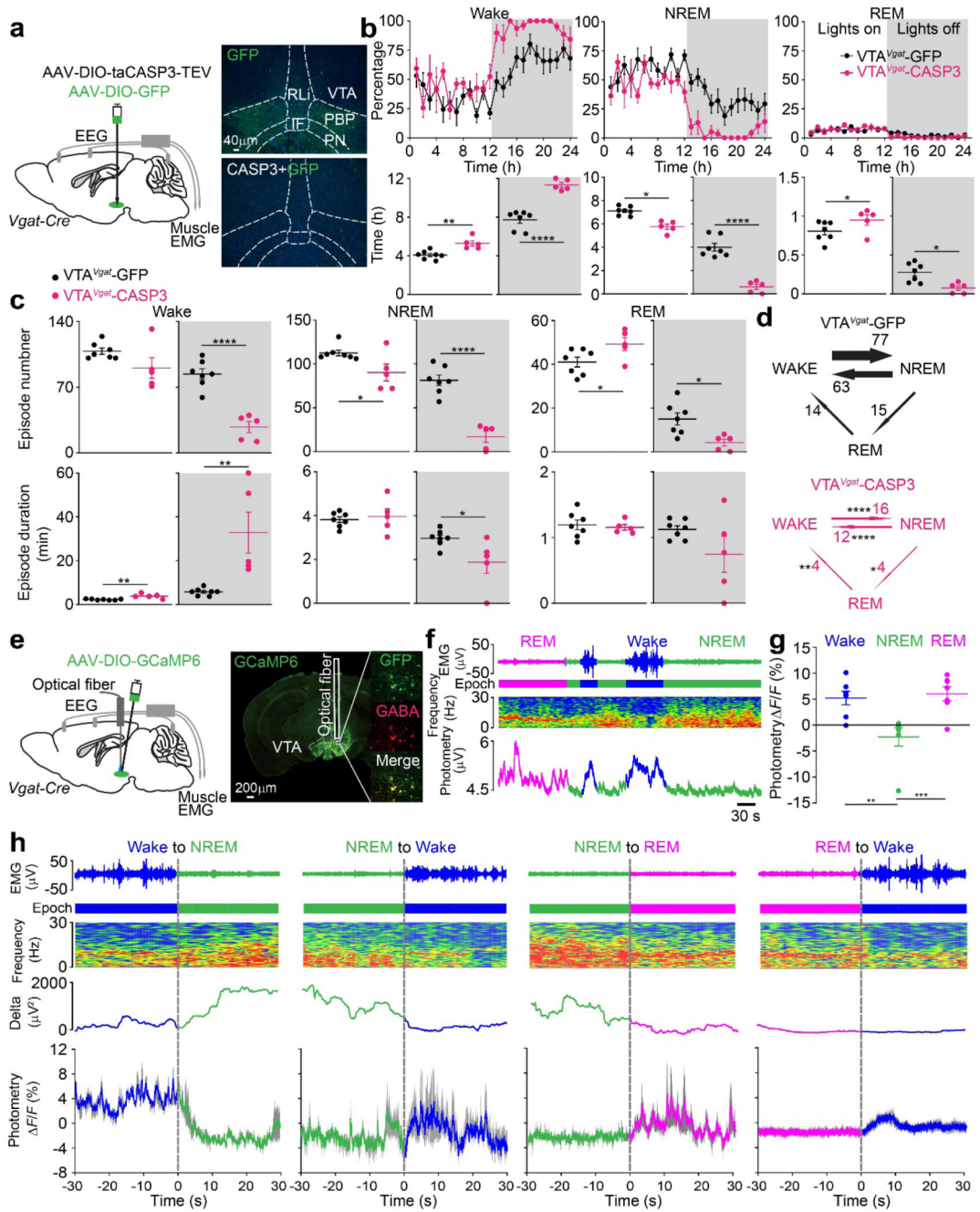


Fig. 6. VTA^{Vgat} neurons inhibit wakefulness. Lesioning of VTA^{Vgat} neurons produces extended wakefulness, but VTA^{Vgat} neurons are selectively wake- and REM-active.

(a) Lesioning of VTA^{Vgat} neurons. Injection of AAV-DIO-GFP (control) or AAV-DIO-taCASP3-TEV into the VTA area of *Vgat-ires-Cre* mice. Pictures show GFP control expression in the VTA area of VTA^{Vgat_GFP} mice and that this GFP expression has been greatly diminished in the caspase treated mice. The experiment was repeated independently 5 times. IF, interfascicular nucleus; PBP, parabrachial pigmented nucleus; PN, paranigral nucleus; PBP, parabrachial pigmented nucleus; RLi, rostral linear nucleus

- (b) Lesioning of VTA *Vgat* neurons increases wakefulness. Percentage of wake, NREM and REM sleep in control VTA *Vgat*-GFP mice (n=7 mice) and VTA *Vgat*-CASP3 mice (n=5 mice), and the total vigilance times in the “lights on” and “lights off” periods.
- (c, d) Lesioning of VTA *Vgat* neurons reduces the transitions between vigilance states and stabilizes wakefulness. Episode number and duration for wake, NREM and REM sleep, and vigilance state transitions during the “lights off” periods in VTA *Vgat*-GFP control mice (n=7 mice) and VTA *Vgat*-CASP3 mice (n=5 mice).
- (e) Fiber photometry for Ca^{2+} levels in VTA *Vgat* neurons. Injection of AAV-DIO-GCaMP6 into the VTA of *Vgat-ires-Cre* mice. GCaMP6 expression can be detected in the VTA area and was co-stained with GABA. The trace of where the optical fiber was placed is illustrated. The experiment was repeated independently 7 times.
- (f) Fiber photometry for VTA *Vgat* neurons. Neurons are more active in wake and REM sleep. Ca^{2+} photometry spectra (bottom trace) recorded in the VTA of VTA *Vgat*-GCaMP6 mice aligned with the EEG spectra (middle trace) and EMG (top trace) during wakefulness, NREM and REM sleep. “Epoch” indicates vigilance state: blue: wake; green: NREM sleep; magenta, REM sleep.
- (g) Fiber photometry for VTA *Vgat* neurons. F/F ratio of the Ca^{2+} photometry signal in VTA *Vgat*-GCaMP6f mice during wakefulness, NREM sleep and REM sleep (n=7 mice; 41 trials).
- (h) Fiber photometry for VTA *Vgat* neurons. Detail of how the Ca^{2+} signal in *Vgat* neurons of VTA *Vgat*-GCaMP6 mice changes at the boundaries of the vigilance states (n=7 mice). “Epoch” indicates vigilance state: blue, wake; green, NREM sleep; magenta: REM sleep. Grey shaded regions represent SEM.
- * $p < 0.05$, ** $p < 0.01$, **** $p < 0.0001$; For b-d, two-sided unpaired t-test, for g, one-way ANOVA. All error bars represent the SEM. For detailed statistics information, see Supplementary Table1.

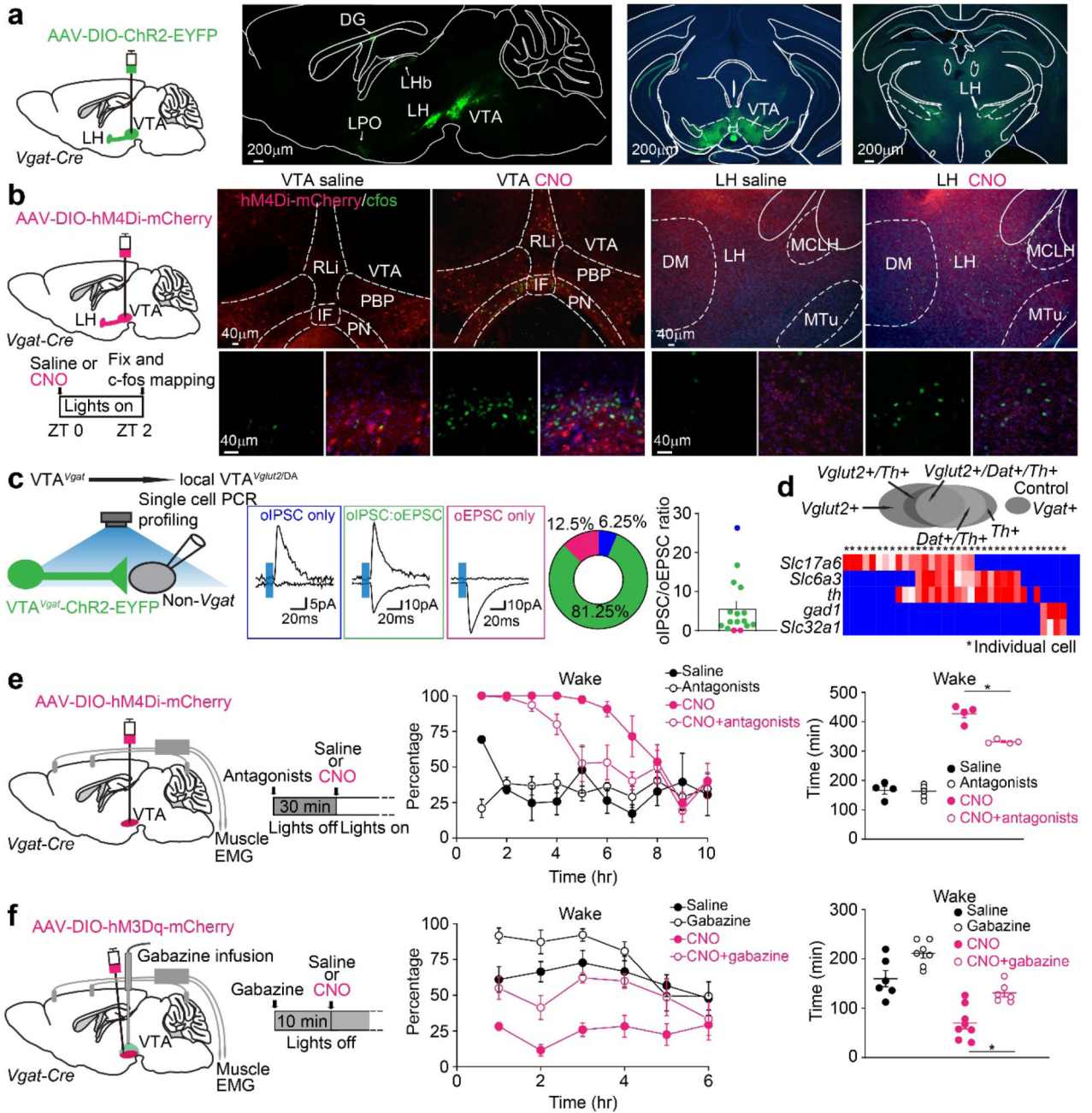


Fig. 7. VTA^{Vgat} neurons limit wakefulness in part by locally inhibiting dopamine and *Vglut2* neurons in the VTA

(a) Mapping axonal projections of VTA *Vgat* neurons. AAV-DIO-ChR2-EYFP was delivered into the VTA of *Vgat-ires-Cre* mice, and axons in the local VTA and projecting to the LH were strongly labelled. The experiment was repeated independently 4 times. DG: detent granule cells; IF, interfascicular nucleus; LH, lateral hypothalamus; Lhb: lateral habenula; LPO: lateral preoptic area; MCLH, magnocellular nucleus, lateral hypothalamus; MTu, medial tuberomammillary nucleus; PBP, parabrachial pigmented nucleus; PN, paranigral nucleus; RLi, rostral linear nucleus; VTA: ventral tegmental area.

(b) cFOS-based activity mapping of brain regions after inhibiting VTA $Vgat$ neurons. In VTA $Vgat$ -hM4D_i mice, cFOS protein expression is found in neurons of the VTA and LH 2 hours after saline or CNO *i.p.* injection at ZT0. The red in the histology figure is the primary fluorescence of the hM4D_i-mCherry-positive axons, the cFOS immunohistochemistry is shown in green. The experiment was repeated independently 6 times.

(c, d) (c) Investigating the local transmitter properties of VTA $Vgat$ neurons in the midline VTA. Acute brain slice electrophysiology was performed on non-Vgat neurons in the midline VTA area in VTA $Vgat$ -ChR2-EYFP mice. Non-Vgat cells were visually selected by YFP negative signals, and after whole-cell status was successfully achieved, a 5ms single blue LED light pulse was given to the local VTA area. The percentages of recorded non-Vgat cells which had either oIPSCs only, or oEPSCs only, or both oIPSCs and oEPSCs were: oIPSC only: 6.25% (n=1); oIPSC and oEPSC (oIPSC: oEPSC), 81.25% (n=13); oEPSC only, 12.5% (n=2). The relative amplitude ratio of the oIPSC peaks versus the oEPSC peaks of non-Vgat cells was 5.71 ± 1.8 (n=16). (d) Heat map for the single-cell PCR of patched cells. The genes tested for were: *Slc17a6* (*vglut2*); *Slc6a3* (*dat*), *Slc32a1* (*vgat*), *th*, and *gad1*.

(e) VTA $Vgat$ neurons inhibit wakefulness in part by inhibiting dopamine neurons. Dopamine receptor D1 and D2/3 antagonists (SCH23390 and raclopride respectively) were injected into VTA $Vgat$ -hM4D_i mice 30 min before saline or CNO injection. Percentage and time of wake was scored after saline or CNO injection (saline: n=4 mice; antagonists: n=5 mice; CNO: n=4 mice; CNO+antagonists: n=4 mice).

(f) Local inhibition from VTA $Vgat$ neurons limits wakefulness. A cannula was placed into the VTA of VTA $Vgat$ -hM3Dq mice and mice were given gabazine 10 min before saline or CNO *i.p.* injection. Percentage and time of wake was scored (saline: n=6 mice; gabazine: n=7 mice; CNO: n=8 mice; CNO+gabazine: n=6 mice).

* $p < 0.05$, for e and f, repeated measures two-way ANOVA and Bonferroni-Holm *post hoc* test. All error bars represent the SEM. For detailed statistics information, see Supplementary Table1.

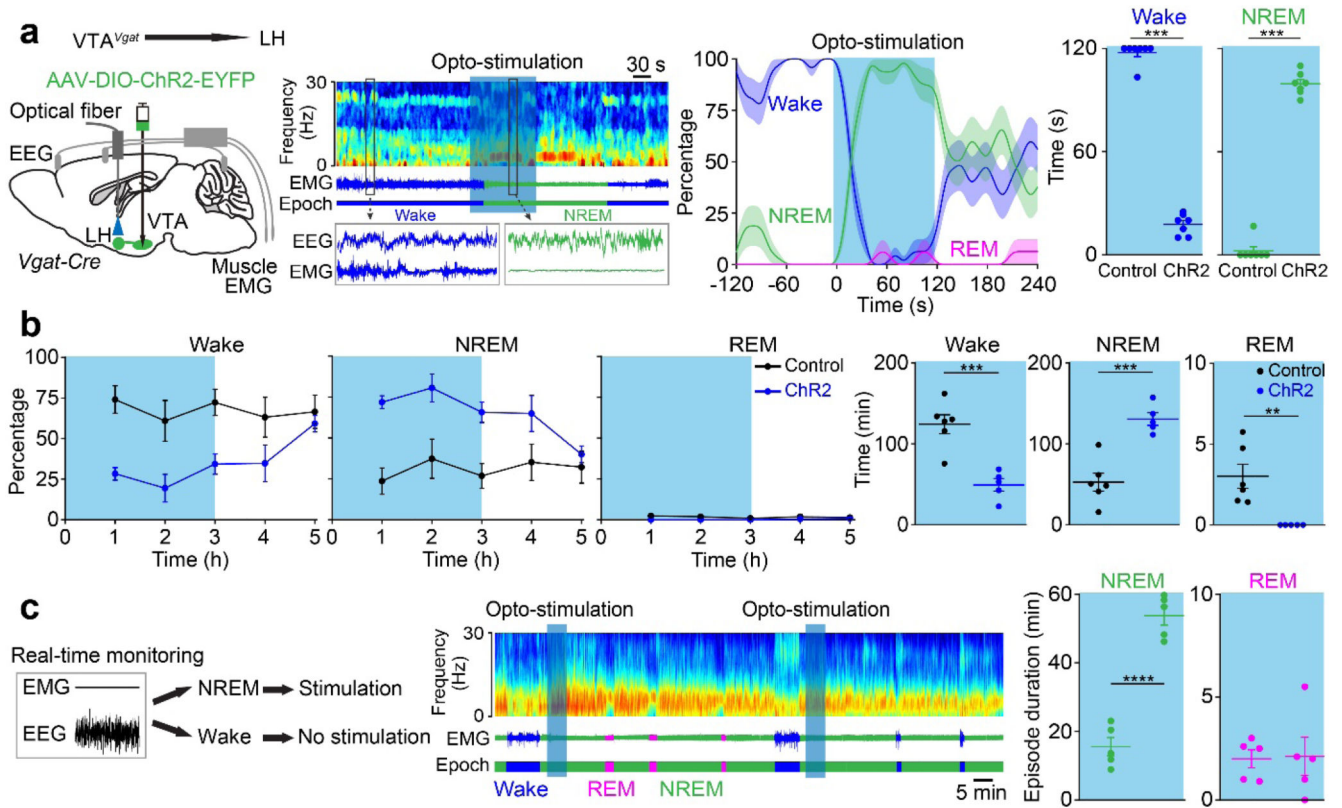


Fig. 8. VTA $Vgat$ neurons inhibit wakefulness in part via projections to the lateral hypothalamus (a, b) To functionally test the VTA $Vgat \rightarrow$ LH projections, an optical fiber was placed into the LH area of VTA $Vgat$ -ChR2-EYFP mice. (a) Mice were given 120 s of opto-stimulation (20 Hz) during their active period (during the “lights off” period) and the percentage and time of wake and NREM sleep were scored (control: n=7 mice; 16 trials; ChR2: n=7 mice; 16 trials) the sem; (b) VTA $Vgat$ -ChR2-EYFP mice (control: n=6 mice; ChR2: n=5 mice) were given 3 hours of opto-stimulation during the active period (“lights-off” period) and the percentage and time of wake, NREM and REM sleep were scored. (c) Mice were given 5 min of opto-stimulation when NREM sleep occurred (control: n=5 mice; 5 trials; ChR2: n=5 mice; 5 trials). The duration of NREM and REM sleep was scored. ** $p < 0.01$, *** $p < 0.001$, **** $p < 0.0001$, for a, two-sided mann-whitney u test. For b and c, two-sided unpaired t-test. All error bars represent the SEM. Shaded regions represent SEM. For detailed statistics information, see Supplementary Table1.